Environmental Research Center Papers

NUMBER 17

1995

Environmental Research Center
The University of Tsukuba

THE EFFECTS OF SOIL MOISTURE ON THE ENERGY BALANCE AT THE BARE SOIL SURFACE*

By Soo-Jin HWANG**

(Manuscript received 31 August, 1995)

ABSTRACT

A knowledge of soil surface thermal properties and an understanding of the interaction between the air and soil surface layer are crucial to improve the performance of current numerical weather forecasting model.

When solar radiation reaches the soil surface, this energy flux is redistributed in the sensible heat flux, latent heat flux, soil heat flux, and long wave radiative energy flux by which the energy balance is maintained.

The relative magnitude of each of these redistributed energy balance components is deeply influenced by the soil surface conditions. For example, the soil surface albedo, the canopy density, and the soil thermal properties such as the soil thermal conductivity or diffusivity are all affected by the soil moisture regime.

In order to study the redistribution of solar energy and energy balance at the soil surface which is affected by the soil thermal properties, field observations were carried out and numerical experiments were conducted by solving the partial differential equation for heat conduction. The field observations took place at the Environmental Research Center of Tsukuba University, Japan during July to August 1982 and July to August 1983.

The results can be summarized as follows;

(1) Soil moisture is evaporated extensively to the atmosphere from the soil surface layer during the daytime, and it is restored from the lower part of soil layer during the nighttime hours. This periodic phenomenon is repeated every day during the drying stage of the soil.

(2) It was found that for the purpose of the numerical experiments the distribution of soil moisture can be assumed to take a logarithmic form as follows.

$$\theta_{w(z,t)} = V_1(t)\log(z) + V_2(t)$$

(3) The vertical gradient of soil temperature in the upper most part of the soil layer becomes gradually steeper in response to the drying process of the soil as the soil moisture becomes depleted. On the other hand, the soil thermal conductivity decreases as the soil moisture decreases. Therefore, on the whole the value of ratio G_0/S_n (soil heat flux at surface / net short wave radiation) may either increase or decrease, depending on the relative importance of the temperature gradient and of the thermal conductivity. Actually, it can usually be assumed that the soil heat flux density is relatively constant, because the high value of the soil temperature gradient and the low thermal conductivity tend to balance each other.

(4) The ratio of the sensible heat flux to net short wave radiation is somewhat small, and it increases little

---

* A dissertation submitted to the Dectoral program in Geoscience, the University of Tsukuba in partial fulfillment of the requirements for the degree of Dector of Philosophy (Science)

**Department of Earth Science, Pusan National University, Jangjeun-Dong Geumjeung-Ku, Pusan, 609−735 KOREA

with decreasing soil water content.

(5) The ratio of the net radiation to the short wave radiation decreases with decreasing soil moisture. This means that the net radiation at the soil surface is deeply influenced by the variation of soil moisture.

(6) A decrease in soil moisture results in an increase of the surface soil temperature and soil surface albedo. As a result, the ratio of net long wave radiation and the net short wave radiation L_n/S_n has a negative correlation with the soil moisture.

(7) The ratio of the latent and sensible heat fluxes has a positive correlation with soil moisture.

(8) The parameter Hr has a negative correlation with the soil moisture. In other words, the ratio of the radiative energy term to the thermo-and aerodynamic heat energy term at the soil surface increases with decreasing soil moisture in the surface soil layer.

(9) The surface albedo of Kanto loam displays a step-like behavior. It has critical points of change from 0.2 to 0.1, between the volumetric soil water contents of 0.3 and 0.2 m^3m^{-3}, respectively.

(10) The results of numerical experiments with Kanto loam suggest that the soil thermal conductivity data of the Kimball (loam, porosity, 0.41) are more representative of the present situation than Kersten's (peat soil, porosity, 0.8).

From the above results, the following conclusions can be drown:

1) There is a low heat conducting layer in the upper most soil layer under dry conditions in the Kanto loam study area. This layer can be defined as a quasi insulated soil layer which is assumed to be developed from the soil surface to lower depth of 0.01 m, and is deepened with drying of soil moisture. The quasi insulated soil layer reveals following characteristics.

(1) The volumetric soil water content in the layer is as small as 0.1 to 0.2 m^3m^{-3}.

(2) The temperature of this layer can change rapidly with rates varying from 5 ℃ h^{-1} to 10 ℃ h^{-1}.

(3) The soil temperature gradient in the layer is usually very steep with typical values of 5×10^2 ℃ m^{-1} to 7×10^2 ℃ m^{-1}.

2) When the soil surface is moist, the incoming solar energy is mainly redistributed into the thermo-and aerodynamic heat flux terms, namely, sensible heat flux, latent heat flux, and soil heat flux. On the other hand, it is mainly transformed into the radiative heat flux when the soil is dry. When the volumetric soil water content at 0.01 m depth varies from about 0.35 m^3m^{-3} to 0.1 m^3m^{-3}, namely, from a wet to a dry state, each component of the energy balance typically varies as follows.

(1) The ratio of net radiation and net short wave radiation Rn/Sn decreases from 0.9 to 0.7.

(2) Both the ratio of sensible heat flux and net short wave radiation H/S_n, and the ratio of the soil heat flux and net short wave radiation G_0/S_n increase from 0.1 to 0.2.

(3) The ratio of latent heat flux and net short wave radiation lE/S_n decreases from 0.6 to 0.3.

(4) The ratio of net long wave radiation and net short wave radiation L_n/S_n increases from 0.1 to 0.3.

(5) The ratio of latent heat flux and sensible heat lE/H which indicates the inverse of the Bowen ratio decreases from 5 to 2.

(6) The parameter H_r which represents the ratio of radiative heat flux term to the thermo-and aerodynamic heat flux term increases from 0.1 to 0.5.

3) In the numerical experiment on soil temperature variation, the soil thermal conductivity and diffusivity are dealt with as functions of soil moisture, which varies with depth and time. The profile of soil moisture can be assumed to be a logarithmic function of depth, that is, the soil moisture increases logarithmically with depth from the soil surface.

The model' s output of soil temperature yields good agreement with the observational results. This confirms the presence of the quasi insulated soil layer in the upper most part of the soil.

CONTENTS

ACKNOWLEDGEMENTS

I would like to thank formally my advisor Dr. Kazuo Kotoda, Professor of the Institute of Geoscience, the University of Tsukuba, without whom this thesis would not have been possible. To share many hours in the office working on our research and to discuss many ideas and concerns outside meteorology has been an outstanding privilege and honor. Dr. Masatoshi M. Yoshino, former Professor of the Institute of Geoscience at Tsukuba University, has always been strongly supportive as my M.S. and former Ph. D. advisor. I would like to express sincere gratitude to Dr. M. Yoshino. I wish to express sincere gratitude to Professor Dr. Isamu Kayane, Professor Dr. Shigemi Takayama, and Professor Dr. Tetsuzo Yasunari, the Doctoral thesis committee members of the Institute of Geoscience at the Tsukuba University for their suggestions and discussions. I would like to express sincere gratitude to Dr. Toshie Nishizawa and Dr. Takeshi Kawamura, former Professors of the Institute of Geoscience at the Tsukuba University for their suggestions. I also wish to thank Professor Dr. Hiroshi Tanaka, Dr. Michiaki Sugita and Dr H. Toritani for their helpful suggestions. In addition, I wish to acknowledge the advice of Professor Wilfried Brutsaert of Cornell University. Finally I would like to thank Dr. S.E. Moon, Professor of the Pusan National University, who introduced me to meteorology.

LIST OF TABLES

LIST OF FIGURES

LIST OF SYMBOLS

Symbol	Description
A	Soil surface albedo
A_{wet}	Albedo at wet soil surface
A_{dry}	Albedo at dry soil surface
c_a	Specific heat of air in soil
c_c	Specific heat of organic matter in soil
c_m	Specific heat of solid soil
C_p	Specific heat of air at constant pressure (1004 Jdeg $^{1}kg^{-1}$)
C_s, $C_{s(z)}$	Soil thermal capacity
$D_{\theta liq}$	Diffusivity of liquid water affected by moisture flux
D_{Tliq}	Diffusivity of liquid water affected by soil temp.
e	Vapor pressure (mb)
F_n	Net long wave radiation
$f(\theta_w)$	Parameter of tortuosity and porosity
G	Soil heat flux density (Wm^{-2})
G_0	Soil heat flux at soil surface
g	Gravitational acceleration at the surface of the earth (9.81 $msec^{-2}$)
H, H_e, H_o	Sensible heat flux density (Wm^{-2})
H_1	Ratio of net long wave radiation to the net short wave radiation
H_2	Ratio of summation H, lE, and G to the net short wave radiation
H_r	Ratio of H_1 to H_2
I	Solar radiation (Wm^{-2})
K_c	Latent heat diffusion coefficient (m^2sec^{-1})
K_h	Sensible heat diffusion coefficient obtained by the eddy correlation method (m^2 sec^{-1})
K_m	Diffusion coefficient of momentum flux (m^2sec^{-1})
K_s	Soil thermal diffusivity
K_w	Hydraulic conductivity
L	Monin-Obuchov length or half number of observed data for Fast Fourier Transform
L_d	Downward long wave radiation flux density (Wm^{-2})
lE	Latent heat flux density
L_n	Net long wave radiation at soil surface
L_u	Upward long wave radiation flux density (Wm^{-2})
m	Number of depth direction in the grid
M_1, M_4	Output voltage of dielectric soil moisture meter subscripts 1, 4 indicates the depth of 0.01 m and 0.04m, respectively
n	Number of time direction in the grid
n_w	Reflection index of water(1.33)
P_0	Atmospheric pressure at ground surface in mb
q	Specific humidity ($kgkg^{-1}$)
q_θ	Soil moisture flux
$q_{\theta,liq}$	Moisture flux of liquid

$q_{\theta,vap}$	Moisture flux of vapor
R_n	Net radiation flux density (Wm^{-2})
S_d, S_u	Downward short wave radiation, and upward short wave radiation reflected by the soil surface
S_n	Net short wave radiation
T_a	Air temperature (℃)
T_s	Soil temperature (℃)
T_0	Soil surface temperature (℃)
T_{10}, T_{45}, T_{80}	Air temperature observed at 0.1, 0.45, and 0.8 m height above the ground, respectively
U	Wind velocity ($msec^{1}$)
u_*	Frictional velocity ($msec^{-1}$)
$u'w'$	Momentum flux (m^2sec^{-2})
V	Volume of sampled soil
$V_1(t)$, $V_2(t)$	Coefficients of logarithmic function for estimation of soil moisture
W_s	Mass of sampled soil
$w'T'$	Thermal flux ($msec^{-1}$℃)
W_t	Total mass of wet soil
W_w	Mass of water in sampled soil
z, z(i)	Depth or height
$\alpha_{(z)}$	parameter for numerical simulation
β	Bowen ratio
ε_a	Emissivity of air
ε_s	Emissivity of soil surface
θ	Parameter for numerical simulation
θ_w	Volumetric soil water content
θ_a	Volume fraction of air in the soil pore
θ_c	Volume fraction of organic matter in the soil
θ_m	Volume fraction of solid soil
θ_1, $\theta_{w(1,t)}$	Volumetric soil water content at 0.01 m depth
θ_{w2}	Volumetric soil water content at 0.02 m depth
θ_4, $\theta_{w(4,t)}$	Volumetric soil water content at 0.04 m depth
$\theta_{w(99,t)}$	Volumetric soil water content at 0.99 m depth
θ_T	Potential temperature (℃)
κ	Von Karmann constant (0.4)
λ, $\lambda_{(z)}$	Soil thermal conductivity at depth of z
λ_{Ki}	Soil thermal conductivity suggested by the Kimball et al. (1976)' s results
λ_{Ke}	Soil thermal conductivity suggested by the Kersten(1946)' s results
ζ	Atmospheric stability
ρ_a	Density of air (kgm^{-3})
ρ_c	Density of organic matter in soil
ρ_m	Density of solid soil
ρ_s	Density of soil
ρ_w	Density of liquid water
ρ_v	Density of water vapor in soil pore

σ	Stefan-Boltzmann constant
σ^n	parameter for numerical simulation
ϕ, ϕ_m, ϕ_h	Universal function of air stability of momentum flux and thermal flux
ϕ_w	Metric tension of liquid water

CHAPTER 1

INTRODUCTION

1.1 Review of recent studies on soil moisture and boundary layer meteorology

Numerous researchers, not only micro-meteorologists but also agricultural meteorologists, or ecologist, have studied interaction processes between soil layer and atmospheric boundary layer (Kuo, 1968; Deardorff, 1978; Schieldge et al. 1982; Mahrer and Segal, 1985; Bristow, 1987; Choudhury and Monteith, 1988; Rakovec and Hocevar, 1988). One reason for the interest is that the accurate values of surface fluxes are required as the initial and the boundary values of a General Circulation Model (GCM) and/or an atmospheric mesoscale circulation model.

In spite of these studies, there still remains several problems in the energy balance of the surface layer which plays an important role in the determination of the surface temperature. For example, it is necessary to know the exact amount of soil moisture in order to fully understand the formation of the surface temperature; unfortunately this problem has been not studied sufficiently.

Daily variations of the air and soil temperature are greatly influenced by the re-distribution of solar radiation. The manner of re-distribution brings an immediately result on the values of sensible, latent, soil heat flux, and long wave radiation. The each term of energy balance components is intend to be a equilibrium state in an instant. As a result, under the conditions of a horizontally homogeneous and a steady state, a energy balance equation is expressed as follows;

$$R_n = H + lE + G \tag{1.1.1}$$

$$R_n = (1 - A)S_d - (L_u - L_d) \tag{1.1.1a}$$

$$H = -C_p\rho_a K_h(\partial T_a/\partial z) \tag{1.1.1b}$$

$$lE = -l\rho_a K_e(\partial q/\partial z) \tag{1.1.1c}$$

$$G = -\lambda(\partial T_s/\partial z) \tag{1.1.1d}$$

where R_n, H, lE, and G indicate the net radiation, the sensible heat flux, the latent heat flux, and soil heat flux, respectively. A, S_d, L_u, and L_d are the soil surface albedo, the downward short wave radiation, the upward long wave radiation, and down ward long wave radiation, respectively. C_p, ρ_a, K_h, K_e, T_a, and z are the specific heat of dry air at constant pressure, the air density, the diffusivity of sensible heat flux, the diffusivity of latent heat flux, the air temperature, and depth, respectively. λ and T_s indicate the soil thermal conductivity and soil temperature, respectively.

On the other hand, the air and soil temperature are represented as follows;

$$C_p\rho_a(\partial T_a/\partial t) = \partial H/\partial z + \partial lE/\partial z + \partial F_n/\partial z \tag{1.1.2}$$

$$C_s\rho_s(\partial T_s/\partial t) = \partial G/\partial z \tag{1.1.3}$$

where C_s, ρ_s, and F_n are the soil heat capacity, soil density, and the net long wave radiation flux, respectively.

To investigate the effect of precipitation on the air and soil temperature, each term of equation (1.1.2) and (1.1.3) will be carefully determined. If the solar radiation, which is independent of soil moisture condition, is given, the net radiation Rn may be decided by the values of soil surface albedo A, up and down ward long wave radiation, L_u and L_d. The soil surface albedo is defined as follows;

$$A = S_u/S_d \tag{1.1.4}$$

where S_u is the reflected short wave radiation by the soil surface. The value of surface albedo A is affected by the soil surface condition such as the soil moisture, soil color, and soil components. However, in this study, soil moisture was merely described as only wet or dry state for the first observation period. The variation of soil surface albedo due to the change of soil moisture has been discussed by Graser and Bavel (1982), and Idso et al. (1975). The terms of the upward and downward long wave radiation flux, L_u, L_d were described in detail by Brunt (1932). L_u can be given as follows;

$$L_u = \varepsilon_s \sigma T_0^4 \tag{1.1.5}$$

where ε_s, σ and T_0 indicate the emissivity of soil surface, the Stefan-Boltzmann constant and soil surface temperature. L_u is a function of the surface temperature which depends strongly on the amount of soil moisture. L_d has been formulated as follows;

$$L_d = \varepsilon_a \sigma T_a^4 \tag{1.1.6}$$

where ε_a is the emissivity of atmosphere which is the function of the water vapor pressure. Because of the fact that water vapor pressure in the atmosphere concern with the soil surface wetness, the downward long wave radiation is also a function of soil moisture. The sensible heat flux is determined by the two terms, i.e., the diffusion coefficient, K_h and the air temperature gradient, $\partial T_a/\partial z$, which are denoted in the equation (1.1.1b). The value of K_h is given as follows;

$$K_h = \kappa u_* z/\phi(\zeta) \tag{1.1.7}$$
$$\zeta = -z/L \tag{1.1.8}$$
$$L = -C_p \rho_a u_* H_0/\kappa g T_0 \tag{1.1.9}$$

where κ, u_*, ϕ and ζ are von Karmann constant (0.4), frictional velocity, the universal function on atmospheric stability, and the stability parameter. H_0, g, L are the sensible heat flux at the soil surface, gravitational acceleration and Monin-Obukhov length. Since H_0 and T_0 also varies with soil moisture, sensible heat diffusivity K_h in equation (1.1.1b) should be changeable with the soil moisture condition. It is clear that the latent heat flux is affected by the evaporation condition of soil, i.e., whether the soil surface is wet or not.

The soil temperature and soil moisture are related as follows (Philip, 1957);

$$\partial\theta_w/\partial t = -1/\rho_w \cdot \partial q_\theta/\partial_z \tag{1.1.10}$$
$$\partial T_s/\partial t = -1/C_s \cdot \partial G/\partial z \tag{1.1.11}$$

where θ_w, ρ_w, q_θ, and C_s are the volumetric soil water content, density of liquid water, soil moisture flux, and volumetric soil heat capacity, respectively. The moisture flux which includes the vapor and liquid types of water and the heat flux are given as follows;

$$q_\theta = q_{\theta,liq} + q_{\theta,vap} \tag{1.1.12}$$
$$G = -\lambda \cdot \partial T_s/\partial z + lq_{\theta,vap} \tag{1.1.13}$$

where $q_{\theta,liq}$, $q_{\theta,vap}$ are the moisture flux of liquid, the moisture flux of vapor, respectively. The moisture flux of liquid is denoted as follows;

$$q_{\theta,liq} = -\rho_w D_{\theta liq} \cdot \partial\theta_w/\partial z - \partial_w D_{Tliq} \cdot \partial T_s/\partial z - \rho_w K_w \tag{1.1.14}$$

where $D_{\theta liq}$ and D_{Tliq} are the diffusivity of the liquid water. These values of diffusivity can be given as follows;

$$D_{\theta liq} = K_w \cdot \partial\phi_w/\partial\theta \tag{1.1.15}$$

$$D_{Tliq} = K_w \cdot \partial\phi_w/\partial T \tag{1.1.16}$$

where K_w and ϕ_w are the hydraulic conductivity and the metric tension of liquid water, respectively. The water vapor flux is represented as follows;

$$q_{\theta vap} = -D_{atm} \cdot f(\theta_w) \cdot \partial\rho_v/\partial z \tag{1.1.17}$$

where D_{atm}, $f(\theta_w)$, and ρ_v indicate the diffusivity of water vapor in air, tortuosity and porosity parameter, and the water vapor density in soil pore, respectively.

The numerical formulae introduced by Philip (1957) have been widely used in numerical experiments, e.g., Sasamori (1970) and Kondo et al. (1992). However, these approaches are not without difficulties. Notably, the diffusivity of equations (15)−(17) varies greatly depending on place, and it is very difficult to determine the exact value by observation.

1.2 Purposes of the study

The field observation and the numerical experiment are carried out to investigate the effect of soil moisture on the surface temperature and the energy balance at soil surface.

To investigate the interaction relationship between the observed values, we carry out the time-series analysis about the air and soil temperature, precipitation, soil moisture, and each component of energy balance.

In Chapter 1, at first we investigate the preceding papers which deal with the effect of soil moisture from a view of boundary layer meteorology. Secondary we point out several unsolved problems of the preceding researches and propose the purposes of the study.

In Chapter 2, the outlines of the observational system in connection with the each terms of energy balance and the calibration of instruments are described. We analyze the observed data for time series analysis to get a relation between the soil temperature and soil moisture.

In Chapter 3, the time variation of the soil moisture is described. Also the relation between the soil heat flux and vertical gradient of soil temperature is described. We write about the soil surface albedo, sensible heat flux, diffusivity of sensible heat flux, and quasi insulated soil layer.

In Chapter 4, numerical experiment is carried out. One dimensional heat transfer equation is used in the experiment. The initial and the boundary condition are given from the observed data. The soil thermal conductivity and diffusivity are considered as a function of soil moisture. The interpolation values of the amount of soil moisture are given by the analysis of Fast Fourier Transform (FFT).

CHAPTER 2

FIELD OBSERVATIONS

2.1 Instrumentation and acquisition of data

The observation site which occupied the area of 400 m^2 had been plowed carefully to form a uniform soil surface before the instruments were installed. Furthermore, in order to obtain the stable condition of soil layer, the site was left untouched for about one month after placing the dielectric soil moisture meters, soil heat flux plates, and thermocouple thermometers in the soil. The surface condition of bare soil was continuously maintained through the observation periods. The period spans from July to August 1982 for the first run, from July to August 1983 for the second run of the experiment. Table 1 lists the meteorological and hydrologic elements measured during the experiment, and schematic view of instrumentation is given in Figure 2.1.1.

Observation levels of dry and wet bulb temperature were 0.1, 0.45, 0.8, 1.6, and 2.7 m above the ground and the thermocouples to measure the soil temperature were buried at 0.001, 0.01, 0.02, 0.03, 0.05, 0.07, 0.1, 0.2, and 0.5 m depth. The installation depths of soil heat flux plates to measure the soil heat flux were 0.01, 0.03, and 0.07 m for the first run period, and 0.01, 0.03, 0.1 m for the second run period.

Generally, Gill type anemometer or 3-cup anemometer is not reliable for measuring the under range of wind velocity of 0.5 m/sec because of its inertia of anemometer (Hayashi and Hwang, 1981). However, since the lower limit of wind velocity detected by sonic anemometer thermometer is above 0 m/sec, sonic anemometer thermometer was installed at 0.45 m height to measure the thermal flux $\overline{w'T'}$ and momentum flux $\overline{u'w'}$ where w', u', and T' are the deviation from the fluctuating value of vertical and horisontal wind components and of air temperature, respectively. It shows that diffusion coefficient, which is related to sensible heat flux and latent heat flux, around 0.45 m height is very differ-

Table 1. Instruments used for the micro-meteorological observations

observation components	device and sensor(type)	remark
air and soil temperature	copper-costantan thermocouple	thickness 0.3 mm
soil moisture	dielectric soil moisture meter (DIK-E) and auger type soil sampler	DAIKI Co. (JAPAN)
soil heat flux	soil heat flux plate (CN-81)	EKO Co. (JAPAN)
net radiation	net radiometer (CN-11)	EKO Co. (JAPAN)
albedo and solar insolation	pyranometer (MR-21)	EKO Co. (JAPAN)
wind velocity and direction thermal and momentum flux	sonic anemometer thermometer (DAT-310)	KAIJO DENKI Co. (JAPAN)
precipitation	rain gauge	data of ERC
evaporation	weighing lysimeter	data of ERC

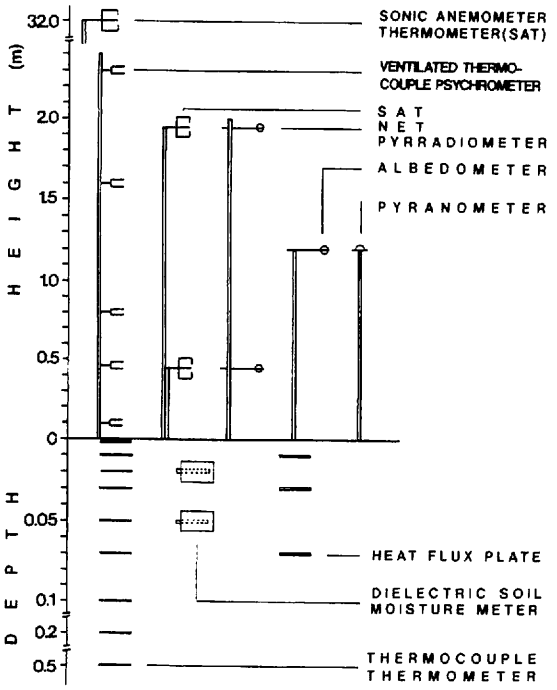

Figure 2.1.1 Schematic diagram of micro-meteorological observation system to measure the energy balance components and soil moisture.

ent from that of upper height's because of steep temperature gradient near the bare soil surface. For reference, the data of sonic anemometer thermometer at 32 m height was obtained from the routine data measured and recorded at some 100 m west of the observation site at the Environmental Research Center (ERC) of the University of Tsukuba.

Two probes of a dielectric soil moisture meter were located at 0.02 m and 0.05 m depth for the first run period, and at 0.01 m and 0.04 m depth for the second run period. To measure albedo on the bare soil surface, two pyranometers were installed both upwards and downwards at 0.45 m height. A Funk type Net radiometer was placed at 0.45 m height as well. Some examples of height placement of net radiometer, for instance, have been 0.1 m by van Bavel and Fritschen (1965); 0.5 m by Rosenberg (1966), Idso and Cooly (1971), and Stanhill, Hofestede, and Kalma (1966); 1.0 m by Davies and Buttimor (1969); 2.0 m by Begg et al. (1964). In the above studies, no reason was given for the height placement of net radiometers. Only Idso and Cooly (1971) suggested that the height placement of net radiometer was 0.5 m above the ground surface because of prevention the effect of ambient air layer between the soil surface and net radiometer. In this study, 0.45 m was adopted for measurement of net radiation.

The sensor for measuring the dry and wet bulb temperature was manufactured to be inserted into the shield with the ventilation device which provides the wind velocity of 3 m/sec or more in order to prevent the radiative heat flux from the sky and from the ground surface (Figure 2.1.2).

Excluding the wind data and temperature components from the sonic anemometer thermometer, other analogue signals of thermocouple thermometers, soil moisture meters, and soil heat flux plates were printed out by using data logger (type YODAC-8), and which were used as an input for computer analysis.

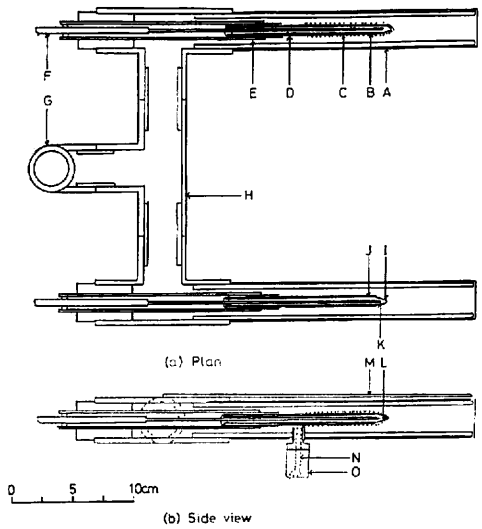

Figure 2.1.2 Diagrammatic cross sections of the ventilated thermocouple psychrometer.
Notation: A, Aluminum sheet;B, wet bulb; C, cotton D, polypropylene pipe; E, plastic pipe; F,lead wire G, vinyl chloride pipe to ventilation manifold; H, vinyl chloride pipe; I, glass; J, dry bulb; K, thermocouple; L, liquid paraffin; M, shelter ;N, vinyl pipe; and O, water reservoir

Sampling intervals of the analogue data were selected as 1 minute or 10 minutes. MELCOM-70 type computer of ERC was used for the analysis of the data obtained at the first observation period and IBM compatible personal computer for the analysis of the second observation period.

The output values of sonic anemometer thermometer, u'w' and w'T' were processed by 10 minutes' running average, which was recorded at the cassette tape recorder at every ten minutes and it was calculated by the MELCOM-70 computer.

2.2 Calibration of instruments

2.2.1 Dielectric soil moisture meter

General methods for determining the soil moisture in situ, include gravimetric, nuclear, electromagnetic, tensiometric, and hygrometric approaches (Schmugge et al. 1980). Of these techniques the electromagnetic and gravimetric methods were used in this study in order to measure the soil moisture continuously and with sufficient accuracy. Since the dielectric soil moisture meter is the equipment which gives the dielectric capacity of soil particles and soil moisture as a voltage, it is necessary to convert the output voltage into the volumetric soil water content.

The dielectric soil moisture meter with two sensors allowed a continuous measurements of the soil moisture. The soil moisture meter does not yield the absolute soil water content, rather it gave a relative value. Therefore the soil samples obtained by auger method has been used to convert the output value of the dielectric soil moisture meter into the volumetric soil water content. The relation between the output value and volumetric soil water content was obtained by the linear regression. Sampling of

the soil was carried out at 0.01−0.035 m, and 0.035−0.06 m depth for the first observation period and 0.0−0.025 m, and 0.025−0.05 m for the second observation to calibrate the output of the dielectric soil moisture meter into the volumetric soil water content.

The soil samples were taken within the 2 m distance around the dielectric soil moisture meter probe by an auger type soil sampler three times a day (9 hour, 13 hour, 18 hour JST). The dielectric soil moisture meter probe of 0.02 m thickness, as shown in Figure 2.2.1, yields the average value of soil moisture between 0.005 m and 0.025 m depth from the surface with one probe placed at 0.015 m depth, and that between 0.03 m and 0.05 m depth another probe buried at 0.04 m depth. On the other hand, the can used for the soil sampling has the inner volume of 0.000005 m^3 with about 0.05 m diameter and 0.025 m height. Thus, the values of soil moisture determined by the two methods represent slightly different soil layer. In the present study, in order to treat them together without assuming too many assumptions, we define the volumetric soil water content of the first layer (denoted by 0.01 m depth hereafter) which means the mean value of the volumetric soil water content between the soil surface and 0.025 m depth, and the volumetric soil water content of second layer (denoted by 0.04 m depth hereafter) means that of 0.025−0.05 m depth.

The soil sample was first weighed at the wet state (W_t). Then, the weight of soil water (W_w) was determined as the difference between the Wt and the weight of dry soil sample (W_s) which was determined after dry in an oven at 105℃ for one day. The volumetric soil water content can be obtained by the following equation (Kayane, 1980);

$$\theta_w = (W_w/W_s) \times (W_s/V)$$
$$= W_w/V(m^3m^{-3}) \qquad (2.2.1)$$

The relation between dielectric soil moisture meter output, the volumetric soil water content obtained by the auger type soil sampler, and dielectric soil moisture meter sensor's temperature can be expressed by the following equations.

$$\theta_1 = 0.0265 - 0.00056\ T_1 + 0.0438\ M_1 \qquad (2.2.2)$$
$$\theta_4 = 0.124 + 0.00233\ T_4 + 0.0441\ M_4 \qquad (2.2.3)$$

where θ is the volumetric soil water content in unit of m^3m^{-3}, and M is the dielectric soil moisture meter output in millivolts, and T is the temperature of the soil moisture sensor. The subscripts 1 and 4

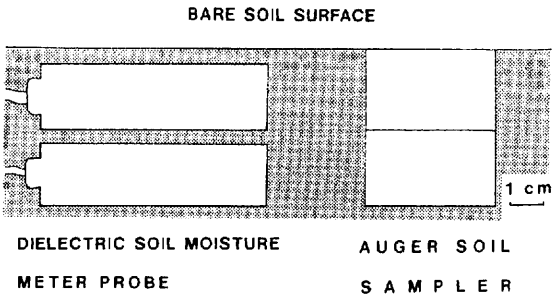

Figure 2.2.1 Schematic diagram for setting the probes of dielectric soil moisture meter and auger type soil sampler in the soil.

represent the depth of 0.01 m and 0.04 m from the soil surface, respectively. Figure 2.2.2 indicates the relation between the dielectric soil moisture meter output M_1 and volumetric soil water content θ_1.

2.2.2 Soil heat flux plate

Three soil heat flux plates were used to measure the soil heat flux in this study. Since there were little difference from one sensor to another in their calibration coefficient and their shape, they were buried at the same depth of 0.02 m for the purpose of inter calibration. Among these three plates, the most reliable one was chosen as a reference and it was used to calibrate two others using the regression line (Figure 2.2.3). The relations are given in the following equations.

$$G_3 = 3.22 + 2.33\ G_1 \quad (r = 0.99) \tag{2.2.4}$$

$$G_3 = 2.00 + 1.11\ G_7 \quad (r = 0.99) \tag{2.2.5}$$

where G is the soil heat flux, subscripts 1, 3 and 7 represent the depth of 0.01, 0.03, 0.07 m from the soil surface, respectively. During the first observation period, the sensors of G_1, G_3, and G_7 were buried at 0.01 m, 0.03 m, and 0.07 m depth, respectively. For the second observation periods, those of G_1, G_2, and G_3 were placed at 0.03 m, 0.01 m, and 0.1 m depth, respectively.

2.2.3 Sonic anemometer thermometer and other instruments

The sonic anemometer thermometer was serviced several times during the experiment by Kaijo Denki in order to maintain accurate measurements.

We adopted the latest calibration values provided by the manufacturers for a pyranometer and for net radiometer. The outputs of the copper-constantan thermocouple with 0.3 mm of diameter used to measure the dry and wet bulb temperature were compared with quartz thermometer. However, there was no obvious difference between sensors. Therefore, it was used without correction.

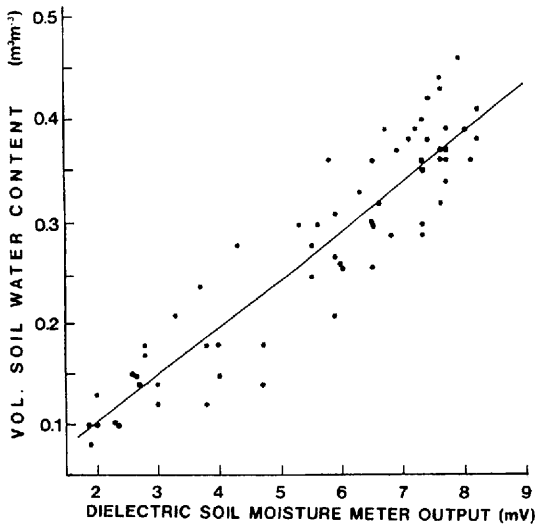

Figure 2.2.2 Relation between the dielectric soil moisture meter output and volumetric soil water content at 0.01 m depth in the soil.

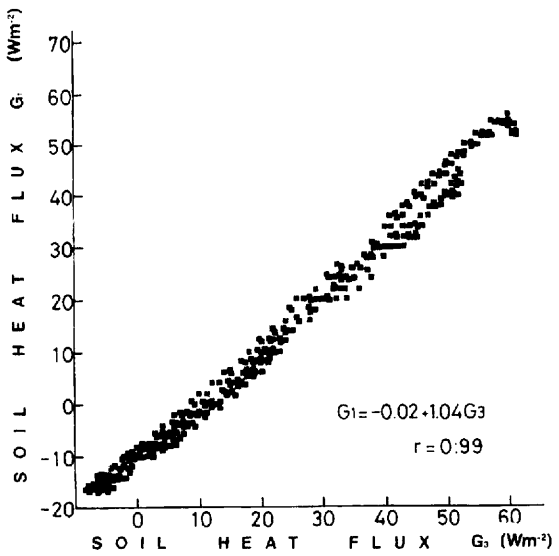

Figure 2.2.3 Relationship between the out put of soil heat flux densities of G_3 and G_1 which were settled at the same depth of 0.02 m for the calibration.

2.3 Air and soil temperature

The changes of air temperature of each level are shown in Figure 2.3.1. There was temperature difference of 2.8℃ between 0.1 m height and 2.3 m height at 13 hour on the 23rd of August. However, the difference of air temperature between the same two levels was below 1℃ at 13 hour on the 13th of September. The similar phenomena such as the above case were also observed in the second observation period.

The difference of soil temperature between 0.01 m depth and surface layer is below 4℃ at 12 hour, the 3rd of August in Figure 2.3.2. But this difference is nearly 10℃ at the same depth in the case of the 9th of August in Figure 2.3.3. Similar to the above case, the gradient of soil temperature in the first observation period in the Figure 2.3.4 got steeper as the volumetric soil water content near surface layer became drier.

We defined the soil condition as the dry condition when the volumetric soil water content of 0.02 m depth in soil was under the 0.1 m^3m^{-3} on the 22nd of August in 1982, and as the wet condition when the volumetric soil water content of 0.02 m depth was over 0.3 m^3m^{-3} on the 13th of September for the first observation period. On the other hand, we defined the soil condition as the dry condition when volumetric soil water content of 0.01 m depth in soil was about 0.1−0.12 m^3m^{-3} on the 9th of August in 1983, and as the wet condition when volumetric soil water content of 0.01 m depth was about 0.3−0.4 m^3m^{-3} on the 3rd of August.

2.4 Wind velocity and related components

2.4.1 Wind velocity

Equation (1.1.1b) and (1.1.7) show that H is a function of stability parameter z/L and diffusion coefficient K_h. Both z/L and K_h are closely related to the wind speed. Thus in order to investigate the

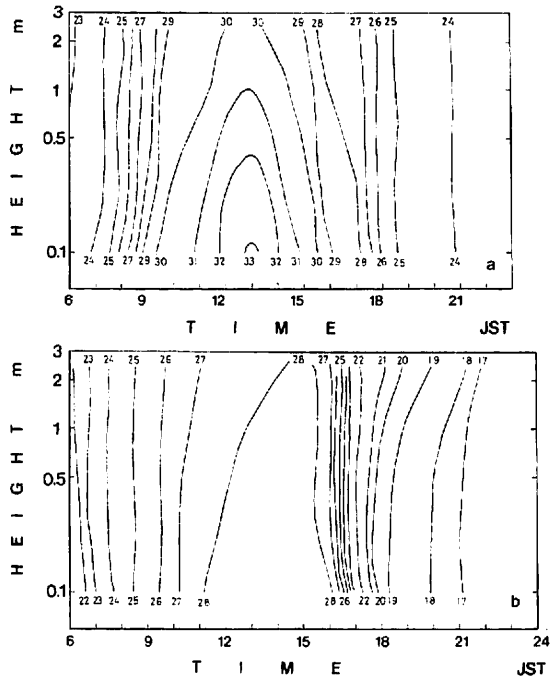

Figure 2.3.1 Height-time variation of air temperature (℃) on August 22, and September 13, 1982 when it reveals the dry state (a) and wet state (b) of soil moisture, respectively.

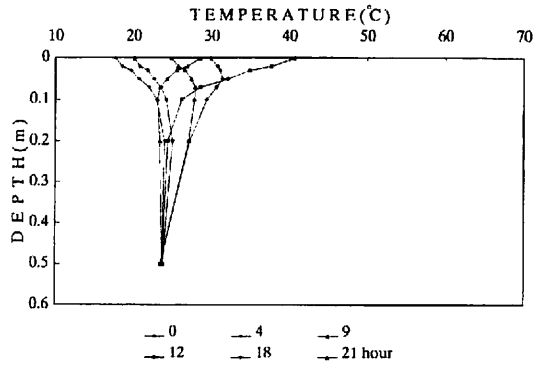

Figure 2.3.2 Diurnal variations of soil temperature profile on August 3, 1983 when it represents the wet state of soil moisture.

behavior of H, it is necessary to look into the wind speed as well. In order to investigate the soil moisture effect on the sensible heat flux density which is concerned with stability parameter z/L and diffusion coefficient of sensible heat, the data of wind velocity at the 0.45 m and 32 m height, which is the lowest measurement height in the surface boundary layer, were analyzed.

Figure 2.4.1 shows the change of wind velocity as a function of time at 0.45 m height and at 32 m

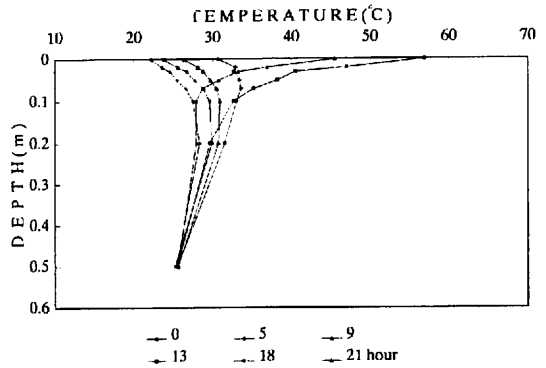

Figure 2.3.3 Diurnal variations of soil temperature profile on August 9, 1983 when it represents the dry state of soil moisture.

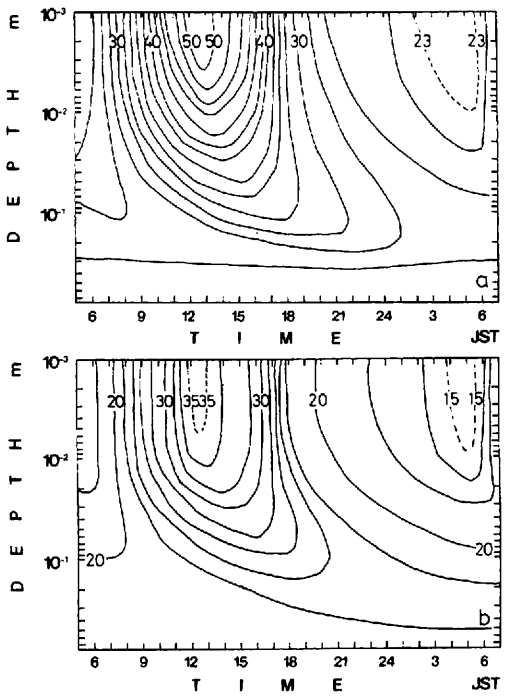

Figure 2.3.4 Depth-time variation of soil temperature on August 22, and September 13, 1982 when it reveals the dry state (a) and wet state (b) of soil moisture, respectively.

height. The wind velocity at 0.45 m height was 1.5−2.0 m/sec during daytime while it was nearly calm during nighttime. At 32 m height, the wind velocity ranged mostly 2−10 m/sec during daytime, and sometimes it 10 m/sec which is beyond the range of the sonic anemometers between the 6th and the 10th of August when the soil was on the dry condition. The range was generally below 1 m/sec at 32 m height during nighttime.

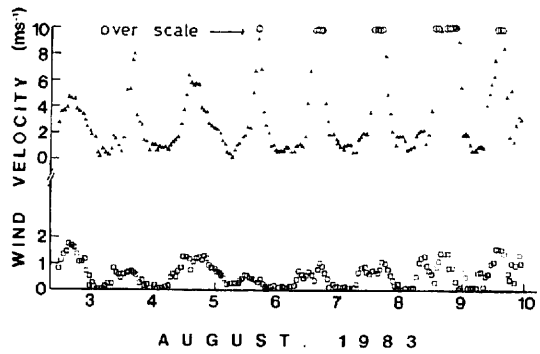

Figure 2.4.1 Daily variation of wind velocity during the second observation period. Open rectangle and closed triangle represent the value at 0.45 m and 32 m height from the ground surface, respectively.

2.4.2 Sensible heat flux density

Sensible heat flux density is the most indispensable component for determining the temperature of surface boundary layer and heat budget of bare soil surface. There are two ways to determine the sensible heat flux density, one of them is an aerodynamic approach which includes an eddy correlation method, a gradient method, and a bulk method. The other is the energy balance method. In the present study, the eddy correlation method was used to determine the sensible heat flux density.

By using the eddy correlation method, sensible heat flux density, He, can be expressed with the following equation;

$$H_e = C_p \rho_a w'T' \tag{2.4.1}$$

where w'T' is the mean thermal flux and is obtained as the production of the vertical wind velocity deviation for the mean value and deviation of temperature from mean value, C_p is the heat capacity of air at constant pressure, and is the density of air expressed with the following equation;

$$\rho_a = 348.38 * P_0/(273.15 + T_{45}) * 0.001 \tag{2.4.2}$$

where the P_0 and T_{45} indicate the atmospheric pressure at ground surface and air temperature at the height of 0.45 m above the soil surface, respectively.

The mean thermal flux density w'T' was obtained by sonic anemometer thermometer.

Figure 2.4.2 illustrates the daily variation of sensible heat flux density which was obtained by the eddy correlation method during the second observation period. The volumetric soil water content at 0.01 m depth was 0.3−0.4 m^3m^{-3} which is wet, on the 3rd and 4th of August, 1983. It reveals 100 W m^{-2} value or so for the daytime and 0−10 Wm^{-2} for the nighttime at wet state of soil. On the other hand, when the soil moisture condition is dry, the sensible heat flux density reveals 130 Wm^{-2} for the daytime, and shows the value −20 Wm^{-2} for the nighttime on the 8th of August, 1983.

2.4.3. Stability parameter z/L

To consider the stability of atmosphere on the diffusion coefficient and sensible heat flux density,

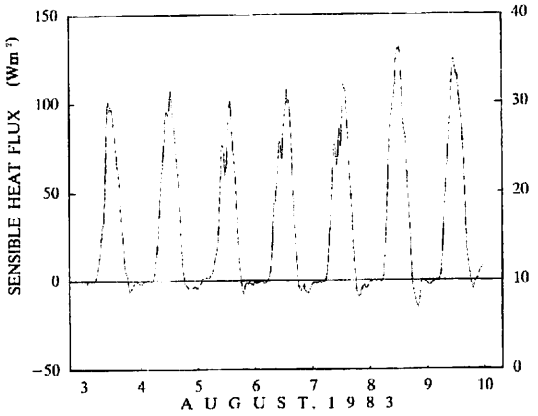

Figure 2.4.2 Daily variation of sensible heat flux density during the second observation period.

sensible heat flux density was obtained from the equation (2.4.1). The friction velocity u_* was obtained as follows:

$$u_* = \sqrt{\overline{u'w'}} \tag{2.4.3}$$

where u'w' is the momentum flux obtained by sonic anemometer thermometer. The atmospheric stability z/L was obtained from the equations (1.1.8), (1.1.9), (2.4.1), and (2.4.3). The heat capacity at constant pressure C_p was set as 1003.0 J/kg/sec in the equation (2.4.1). Air density ρ was defined by the equation (2.4.2).

Figure 2.4.3a,b,c,d shows the time variation of stability parameter z/L. Even z/L is somewhat different through the whole observation period, it is low to the extent of $-0.1 - -0.3$ from 6 hour to 18 hour, that is day time, which indicates the unstable state of atmosphere. Also z/L shows $0.1 - 5.0$ from 18 hour to 6 hour of next day, that is nighttime, which indicates the stable state of atmosphere. However, the atmosphere was almost neutral from 18 hour of the 4th to 6 hour of the 5th in August.

2.5 Precipitation and soil moisture

Clear days prevailed during the period from the 18th to 26th of August, 1982 during the first observation period so that the volumetric soil water content at 0.02 m depth decreased from 0.29 m^3m^{-3} to 0.22 m^3m^{-3}. The soil moisture increased several times by precipitation after that period. There was 100 mm/day of precipitation on September 9, 1982 due to the passing of midlatitude cyclone through the Kanto area of Japan. On this day, the volumetric soil water content at 0.02 m depth reached maximum value of 0.46 m^3m^{-3}. The daily variation of soil moisture at the first observation period is illustrated in Figure 2.5.1.

There was 72.2 mm/day of precipitation due to Baiu front from the 25th to 28th of July, 1983, and it was assumed that there was more than 100 mm/day of precipitation within 24 hours (from the 1st to 2nd of August). At later time the amount of precipitation was not observed because of the power failure at ERC. After that, it was clear until 12th of August so that soil moisture become dry.

The daily variation of volumetric soil water content at 0.01 m and 0.04 m depth is illustrated in

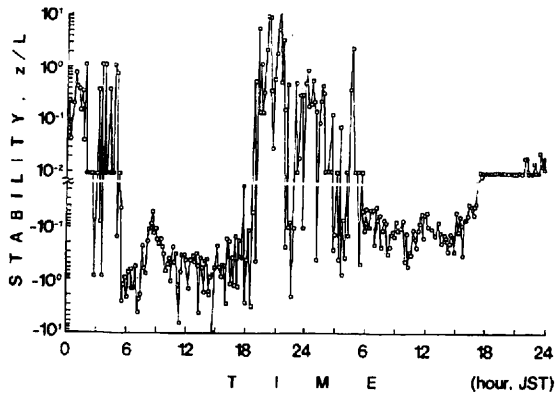

Figure 2.4.3a Time variation of atmospheric stability z/L on August 3−4.

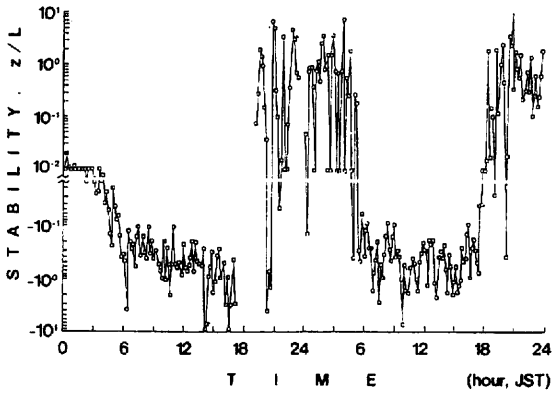

Figure 2.4.3b The same as the Figure 2.4.3a but for August 5−6.

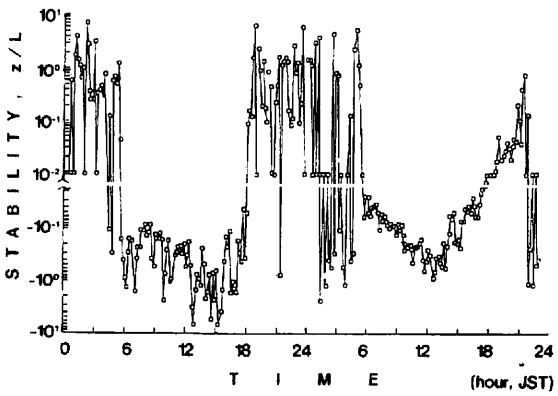

Figure 2.4.3c The same as the Figure 2.4.3a but for August 7−8.

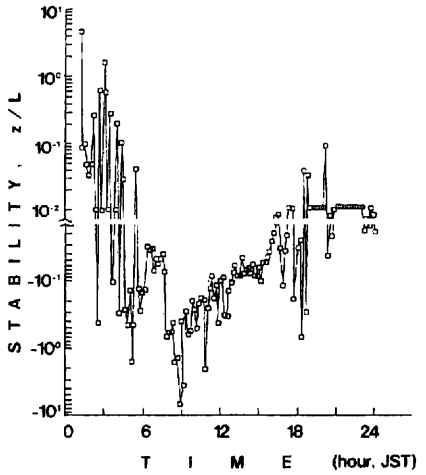

Figure 2.4.3d The same as the Figure 2.4.3a but for August 9.

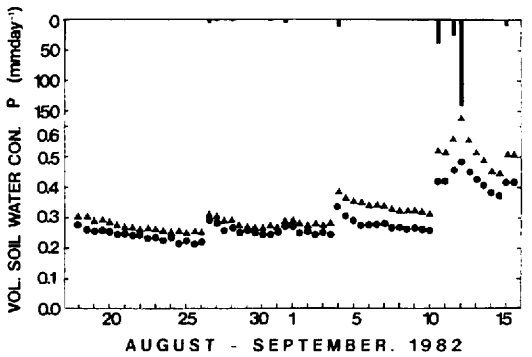

Figure 2.5.1 Variations of volumetric soil water content and precipitation during the first observation period. Closed triangle and circle represents the volumetric soil water content at 0.05 m and 0.02 m depth in soil, and P means precipitation (mm/day).

Figure 2.5.2 from the 2nd to the 12th of August in the second observation period. The volumetric soil water content decreased from 0.4 m^3m^{-3} to 0.1 m^3m^{-3} at 0.01 m depth in soil. It can be seen that daily variation of volumetric soil water content shows daily maximum value at 6 hour and daily minimum value at 15 hour, and that soil moisture decreases from 0.42 m^3m^{-3} to 0.22 m^3m^{-3} at 0.04 m depth during this period. The pattern of drying of soil moisture at 0.04 m depth is similar to that at 0.01 m depth, but its range of daily variation is smaller. Similar result was obtained by Schieldge et al. (1982) in the San Joaquin Valley in California.

In the second observation period, the soil maintained field capacity extending from mid-June to early July due to the continuous rainfall. The volumetric soil water content at 0.01 m and 0.04 m depth came

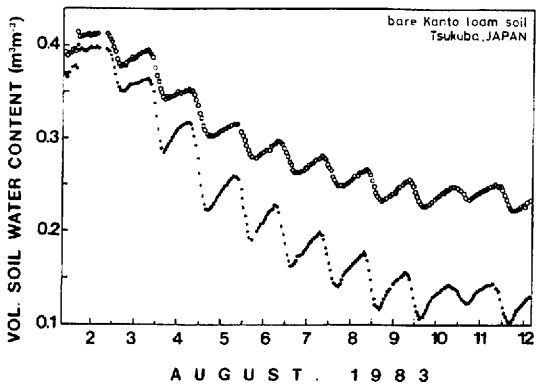

Figure 2.5.2 Variations of volumetric soil water content during the second observation period. Closed and open circle indicate the volumetric soil water content at 0.01 m and 0.04 m depth in soil, respectively.

up nearly field capacity at the 4th of July as shown in Figure 2.5.3. The values were 0.36 m^3m^{-3} and 0.39 m^3m^{-3}, respectively. On the following day of 5th July, the volumetric soil water content at 0.01 m depth increased to 0.42 m^3m^{-3} due to the precipitation of 18.9 mm/day. That of 0.04 m depth increased to 0.55 m^3m^{-3}.

The amount of soil moisture increase at 0.04 m depth was larger than that of 0.01 m depth. This is probably because the soil moisture at 0.04 m reached equilibrium. Similar results were also obtained in the case of the precipitation of 6th and 8th, July. The rainfall continued from 10th to 12th, July with 0.4 mm/day, 0.2 mm/day and 0.7 mm/day, respectively. After two days without rainfall on 13th and 14th July, the soil got wet again with rainfall of 4.8 mm/day on 15th July. The volumetric soil water content at two depths of 0.01 m and 0.04 m slightly decreased with some variation until 12th, July.

The soil moisture at 0.01 m depth decreased much more contrary to the decrease of that at 0.04 m on 13th and 14th, July, 1983 as shown in Figure 2.5.3. From 13th to 14th July, the decrement reached at 0.09 m^3m^{-3}. The volumetric soil water content at two depths of 0.01 m and 0.04 m were nearly equal on 25th, July. Soil moisture increased again to 0.48 m^3m^{-3} (at 0.01 m depth) and 0.69 m^3m^{-3} (at 0.04 m depth) due to the rainfall of 64 mm/day on 28th, July, respectively.

From the variation of the volumetric soil water content, it was found that the maximum volumetric soil moisture content was about 0.7 m^3m^{-3}, which means that porosity of the soil was about 0.8. The volumetric soil water content of about 0.7 m^3m^{-3} decreased to about 0.4 m^3m^{-3} on 29th, July. It is considered that the greater part of decreased amounts penetrated into deeper soil layer. The volumetric soil water content decreased due to clear weather from 3rd to 14th, August.

Generally there is periodically increase and/or decrease of soil moisture, and the phases of daily variation at two depth are similar to each other from 3rd to 7th, August. On the other hand, there are lag of phases at two depth on 8th to 14th, August (Figure 2.5.4). These reveal that there is appearance of quasi insulated layer. This problem will be discussed again in the section of conclusions.

Figure 2.5.5 indicates the daily variations of the rainfall and volumetric soil water content. A heavy rainfall (total, 98.3 mm) occurred from 15th to 18th, August. On the day before the rainfall, the soil at two depths was dry. Owing to rainfall of 36.2 mm/day on 15th, August, they rapidly increased from

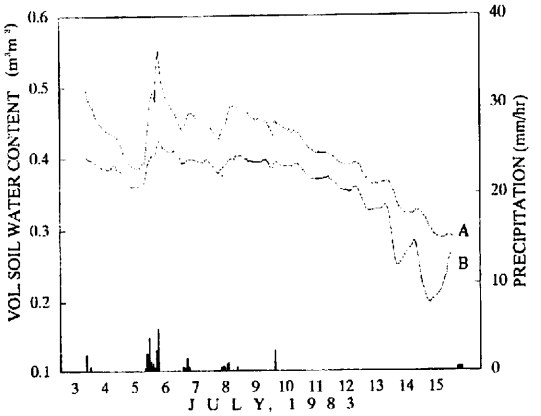

Figure 2.5.3 Daily variations of soil moisture and precipitation on July 3-15, 1983. Line A and line B represents the volumetric soil water contents at 0.04 m and 0.01 m depth, respectively. Bar means the precipitation of an hour mean.

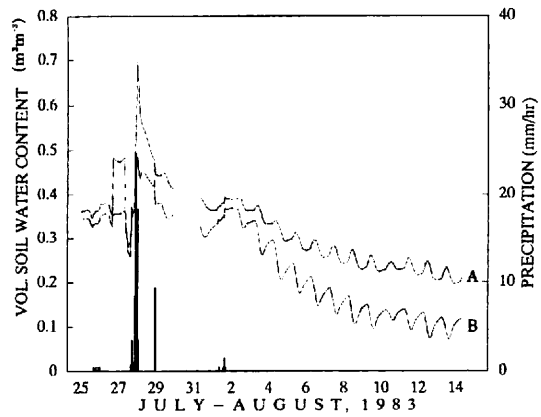

Figure 2.5.4 The same as the Figure 2.5.3 but on July 25 August 14, 1983.

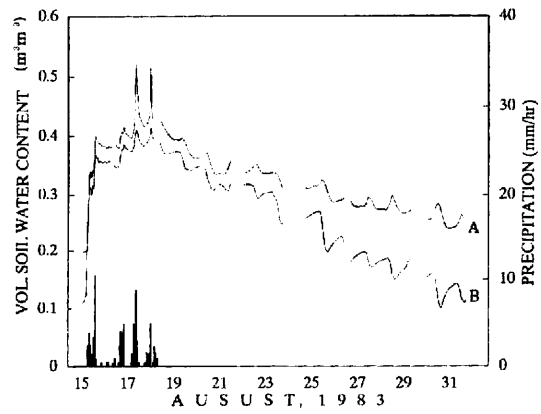

Figure 2.5.5 The same as the Figure 2.5.3 but on August 15−31, 1983.

0.12 m^3m^{-3} at 0.01 m depth and 0.2 m^3m^{-3} at 0.04 m depth to 0.36 m^3m^{-3} and 0.38 m^3m^{-3}, respectively. The maximum value at 0.04 m depth of 0.52 m^3m^{-3} was observed due to the rainfall of 34.7 mm/day on 17th, August.

The soil at two depths was dry until 5 hour 15th, August. The rainfall of 2 $mmhr^{-1}$ from 5 to 6 hour increased the volumetric soil water content to 0.21 m^3m^{-3}. However, that of 0.04 m depth did not change until 6 hour. By 7 hour, those of 0.01 m and 0.04 m depth increased to 0.287 m^3m^{-3} and 0.279 m^3m^{-3}, respectively. After that time, they rapidly increased to 0.31 m^3m^{-3} at 0.01 m and 0.34 m^3m^{-3} at 0.04 m depth by 8 hour, respectively. In response to the rainfall events, soil moisture increased and/or decreased after the time. At the same time of the above, soil moisture of 0.04 m depth which was about 0.02 or 0.03 m^3m^{-3}, was much more than that of 0.01 m depth.

It took about one hour for the rainfall to penetrate down to 0.04 m depth. Once the soil became saturated, the volumetric soil water contents at 0.01 m and 0.04 m depth increased together in proportion to the rainfall. Drying processes on cloudy days were different from those of clear days as shown in Figure 2.5.5 by comparison with Figure 2.5.4.

2.6 Solar radiation and net radiation

Clear days continued in the second observation period after several rainfall events which had fully saturated the soil layer from 3rd to 10th of August 1983. Figure 2.6.1 shows the daily variation of solar radiation and net radiation. The maximum solar radiation of August 3rd was 857 Wm^{-2}, but that of 7th was 679 Wm^{-2}. Five days later from 3rd, solar radiation was increased again to 887 Wm^{-2}. The maximum net radiation of 3rd, August 1983 was 661 Wm^{-2}, while that of 8th August 1983 was 505 Wm^{-2}. This means that the ratio of net radiation to solar radiation decreased. This trend coincides with the decrease of the soil moisture in Figure 2.5.2. Durand et al. (1988) reported similar results, in which the net radiative flux differences were explained by the difference in surface albedo. In the present study, it is important to investigate whether the ratio of net radiation to solar radiation is decreasing or not, because the process of redistribution of the net radiation is very important to the surface energy balance. This problem will be discussed in the next Chapter. Net radiation of nighttime decreased rapidly down to negative value in early evening and then turned positive value again at dawn. Some difference of the minimum values of net radiation can be noticed. The minimum net radiation during

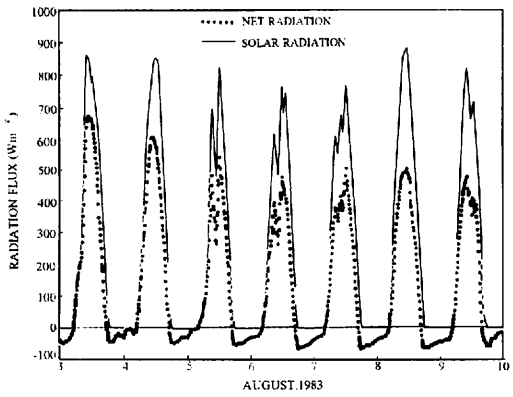

Figure 2.6.1 Daily variation of solar radiation and net radiation on 3−10 August 1983.

nighttime was smaller on the 3rd, 4th and 5th of August than that of the 6th, 7th, 8th and 9th of August. Also, the comparison of the pattern of the variation of the net radiation at around dawn reveals difference concerned with soil wetness (Figure 2.2.3). Because the net radiation balanced by the sensible heat flux, soil heat flux and latent heat flux as shown in equation (1.1.1), these energy balance components should deeply be related to soil moisture conditions.

CHAPTER 3

DISCUSSION ON THE OBSERVATION RESULTS

3.1. Estimation of volumetric soil water content

For the purpose of numerical experiments and the estimation of soil thermal capacity, the volumetric soil water content in the soil layers where measurements are not available was estimated as a function of time and depth as follows. At first, values of θ_w at 0.01 m and 0.04 m depth for a given time were estimated by the Fast Fourier Transform analysis, given bellow, for the data set obtained during the second run period, i.e., from August 3 to August 12.

$$\theta_{w(1,t)} = \frac{A_{01}}{2} + \sum_{n=1}^{L} [A_{n1}\cos(n\pi\frac{t}{L}) + B_{n1}\sin(n\pi\frac{t}{L})] \tag{3.1.1}$$

$$\theta_{w(4,t)} = \frac{A_{04}}{2} + \sum_{n=1}^{L} [A_{n4}\cos(n\pi\frac{t}{L}) + B_{n4}\sin(n\pi\frac{t}{L})] \tag{3.1.2}$$

$$A_{ni} = \frac{1}{L}\int_{-L}^{L}\theta_{wi}(t)\cos(n\pi\frac{t}{L})dt \tag{3.1.3}$$

$$B_{ni} = \frac{1}{L}\int_{-L}^{L}\theta_{wi}(t)\sin(n\pi\frac{t}{L})dt$$

$$i = 1, \tag{3.1.4}$$

where L is the half number of observed data, 108. The value of A_{ni}, B_{ni} are the amplitude of sine and cosine function. A_{01}, A_{04}, are the first term of fourier transform. The n and t are the repeat number and time. Subscript 1 and 4 mean the observed depths at 0.01 m and 0.04 m, respectively. Also it was assumed through the whole observation period that volumetric soil water content at z=0.99 m for all values of t, $\theta_{w(99,t)}$, maintained 0.43 m^3m^{-3}. Once time series of $\theta_{w(1,t)}$, $\theta_{w(4,t)}$ were obtained, a logarithm relation between the depth and the volumetric soil water content at three depths was determined by assuming logarithmical decrement towards the surface layer.

$$\theta_{w(z,t)} = V_1(t)\log(z) + V_2(t) \tag{3.1.5}$$

where $V_1(t)$ and $V_2(t)$ are the time variables which were obtained from the observation value of $\theta_{w(1,t)}$, $\theta_{w(4,t)}$, and the assumption value of $\theta_{w(99,t)}$.

Figure 3.1.1 shows the change of volumetric soil water content estimated by the equation (3.1.5) as a function of depth and time, and it reveals that the water content of surface layer decreases rapidly as the soil becomes dryer. In the Figure 3.1.2, the cross sign and closed circle represent the volumetric soil water content observed at 0.04 m and 0.01 m depth, respectively. The soil moisture of the 21st layer was kept 0.43 m^3m^{-3} through the whole observation period. Daily variation becomes intense towards the surface layer and the minimum value of soil moisture reached 0.03 m^3m^{-3} in the 1st layer. The above result is very similar to the daily change obtained by numerical study of soil moisture suggested by Camillo et al. (1983).

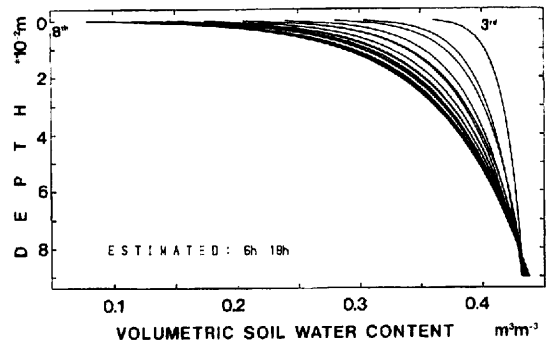

Figure 3.1.1 Profiles of daily estimated volumetric soil water content at 6 hour and 18 hour during 3−12 August 1983.

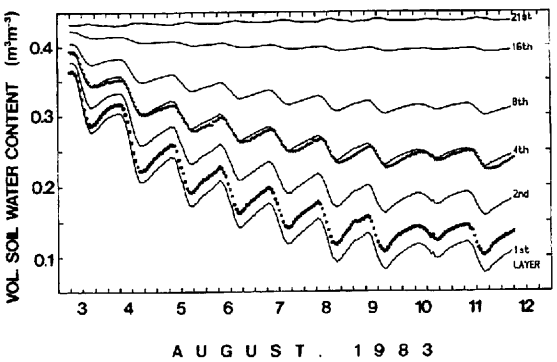

Figure 3.1.2 Estimated and observed volumetric soil water content during the second observation period. The depth of 1st-21st layer is given in Table 2. Crosses and closed circles represent the observed value at 0.04 m and 0.01 m depth, respectively.

3.2 Soil heat flux density and net radiation

The relation between soil heat flux density and net radiation during the first observation period is illustrated as a function of soil wetness in Figure 3.2.1, where open circle represents relationship for the values observed under the soil moisture condition of 0.22−0.25 m^3m^{-3} and closed circle represents that of 0.30−0.44 m^3m^{-3} at the depth of 0.02 m. The experimental equation for each condition was determined as follows;

$$G_1 = -1.5 + 0.15\ R_n,\ 0.22 \leq \theta_w \leq 0.25 \quad (3.2.1)$$

$$G_1 = -2.7 + 0.11\ R_n,\ 0.30 \leq \theta_w \leq 0.44 \quad (3.2.2)$$

As shown in the equation of (3.2.1) and (3.2.2), the gradient of equation becomes steeper as the soil moisture decreases. The relation between the ratio of soil heat flux to net radiation and soil moisture for daytime is illustrated in Figure 3.2.2. The ratio of G_1/R_n was 0.13−0.2 for 0.20−0.26 m^3m^{-3},

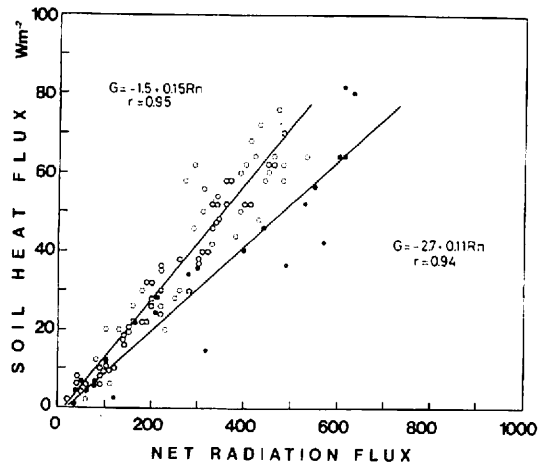

Figure 3.2.1 Relation between the soil heat flux measured at 0.01 m depth in bare soil of Kanto loam and net radiation flux during the first observation period. Open and closed circles indicate those observed when the volumetric soil water content was in the range of $0.22-0.25$ m^3m^{-3} and $0.30-0.44$ m^3m^{-3}, respectively.

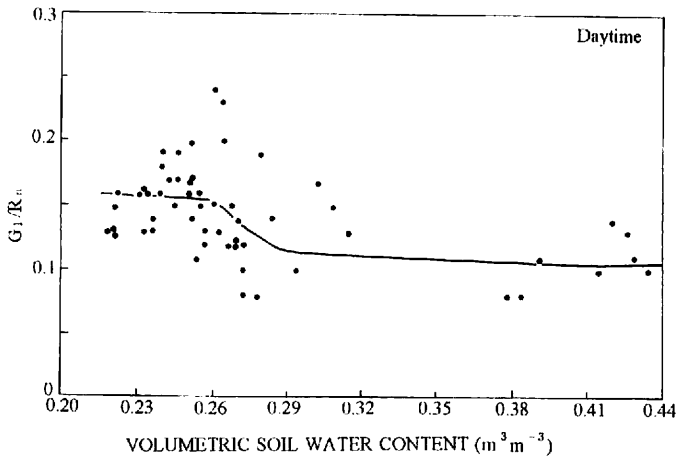

Figure 3.2.2 Relation between the ratio of G_1/R_n and the volumetric soil water content for daytime during the first observation period.

0.1 - 0.15 for $0.26-0.29$ m^3m^{-3} and $0.08-0.12$ for 0.29 m^3m^{-3} or more. This tendency indicates the negative relation between volumetric soil water content and ratio of G_1/R_n. Fig 3.2.3 shows the case of nighttime. The effect of soil moisture is greater for nighttime than for daytime, because the ratio of G_1/R_n increases from 0.15 to 0.7 for soil moisture variation. It is noticed from these results that the effect of soil moisture on the ratio G_1/R_n is larger for nighttime than for daytime and also acts inversely.

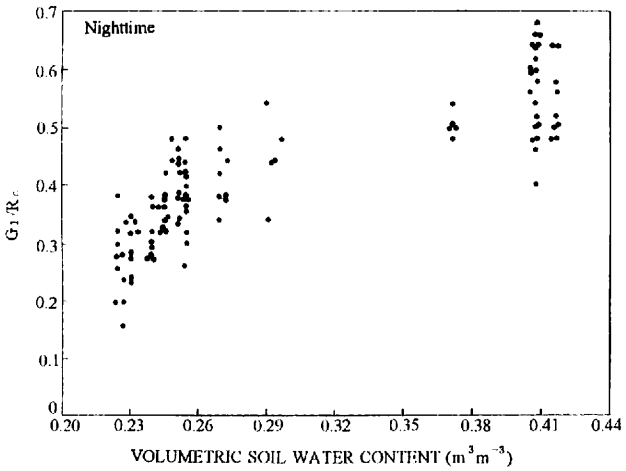

Figure 3.2.3 The same as the Figure 3.2.2 but for nighttime.

3.3 Soil surface albedo and soil moisture

Since the soil surface albedo varies with soil moisture variation, when the energy balance and soil surface temperature variation are discussed, the relation of soil moisture and albedo have to be dealt with together.

The relations are examined by the field observations and by laboratory experiments. Graser and van Bavel(1982) and Kondo et al. (1992) denote the relation of the albedo and soil moisture. On the other hand, Idso et al. (1975) carried out field observation to know the variation of soil surface albedo with soil moisture. All these results revealed a step like function.

To know the relation between soil moisture and albedo at Kanto loam, in this study, data were obtained during the first and second observation.

The albedo of bare soil surface varies continuously in a day. Therefore, the values of albedo which satisfy the following criteria were taken for the analysis. (1) Solar radiative flux was above $400 Wm^{-2}$. (2) When the declination of sun was high, namely, 10−14 o'clock in a day.

The relation between volumetric soil water content and albedo on bare soil surface is given in Figure 3.3.1, which suggests the following result.

1. At the state of dry condition of soil where the volumetric soil water content measured at 0.02 m depth is less than 0.26 m^3m^{-3}, the soil surface albedo is nearly constant and is around 0.14.
2. The soil surface albedo decreases rapidly with the increase of the volumetric soil water content for θ range of 0.26 m^3m^{-3}−0.29 m^3m^{-3}.
3. The albedo is about 0.09 and nearly constant for $\theta > 0.29$ m^3m^{-3}.

From the above observational results, we found that the albedo of bare soil surface had the critical point at 0.26−0.29 m^3m^{-3} volumetric soil water content and varies like a step-like function. The similar results had been reported by Idso et al. (1975) from the field observation (see Figure 3.1.1) and Graser and Van Bavel(1982) from the laboratory experiment. The relation between soil moisture and soil surface albedo was not identified whether it is linear or step-function yet. So the value of the volumetric soil water content was taken at 0.02 m depth during the first observation period, the relation between soil moisture and albedo on the bare soil surface can not be precisely discussed here. However, it should be expressed as a step-like function from the present observational results of albedo and net radia-

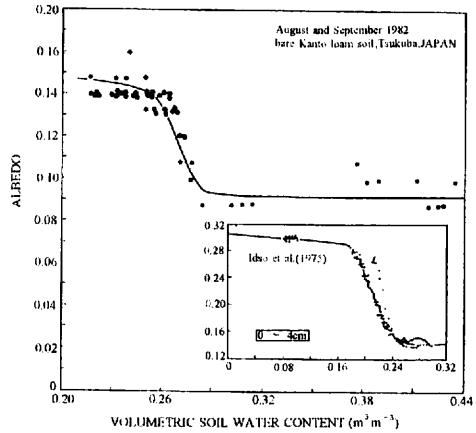

Figure 3.3.1 Relation between the albedo of bare soil surface and volumetric soil water content measured at 0.02 m depth in soil during the first observation period.

tion.

Ångstrom(1925) has suggested the following relation between bare soil surface albedo and wetness of soil.

$$A_{wet} = A_{dry} / [n_w^2(1 - A_{dry}) + A_{dry}] \qquad (3.3.1)$$

where A_{wet} and A_{dry} are the albedo of wet and dry soil in m^3m^{-3} and n_w is the index of refraction of water, usually taken as 1.33. The albedo when volumetric soil water content is in the range of $0.22-0.25$ m^3m^{-3} during the first observation period was considered to be that of dry surface. The albedo $0.15-0.14$ was used as an input for the equation (3.3.1). Then the albedo of wet soil state can be calculated as $0.09-0.084$, which is almost the same value as the observed albedo value of $0.09-0.08$ when the soil was considered to be wet, i.e., when the θ_{w2} was from 0.29 m^3m^{-3} to 0.44 m^3m^{-3}. The equation (3.3.1) suggested by Ångstorm (1925) is reliable to estimate the soil surface albedo from the above results. But the soil condition is not fully classified, more detailed soil moisture condition must be adopted.

Figure 3.3.2 shows the variation of the soil moisture and soil surface albedo during the second observation period. When the soil moisture was more than 0.3 m^3m^{-3} at 0.01 m depth, the albedo of soil surface was about 0.1. When the soil moisture at the depth of 0.01 m decreased to the value of 0.2 m^3m^{-3} or less, the soil surface albedo increased to 0.2.

Figures 3.3.3 and 3.3.4 show the diurnal variation of soil moisture and soil surface albedo. In Figure 3.3.3, when the soil moisture decreased from 0.3 m^3m^{-3} to 0.2 m^3m^{-3}, the soil surface albedo increased from 0.1 to 0.2. On the other hand, the soil surface albedo nearly stayed constant when the soil moisture decreased from 0.2 to 0.1 as shown in Figure 3.3.4. Figure 3.3.5 represents the similar steplike function between the soil moisture and soil surface albedo to the first observation result. In the second observation results, the critical points of variation are at higher value of soil moisture. It is assumed that the soil moisture is taken at more shallow depth on the second observation period than that

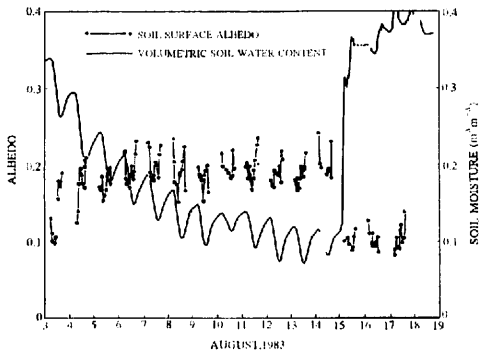

Figure 3.3.2 The daily variations of soil moisture and bare soil surface albedo during the second observation period.

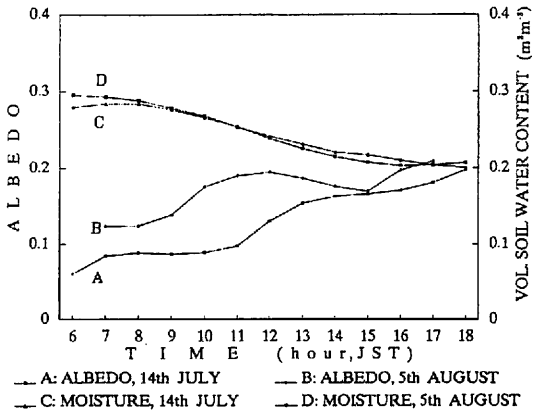

Figure 3.3.3 Diurnal variation of soil moisture and albedo on 5th and 14th August 1983.

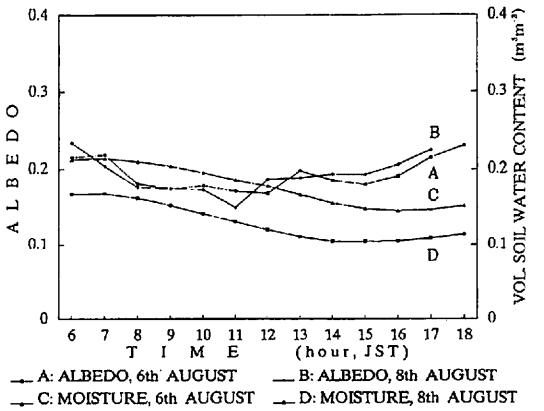

Figure 3.3.4 The same as the Figure 3.3.3 but for 6th and 8th August 1983.

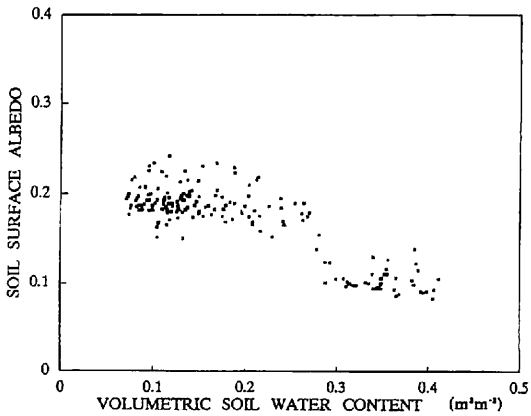

Figure 3.3.5 Soil surface albedo versus volumetric soil water content on second observation period.

of the first observation period.

3.4 Soil heat flux and sensible heat flux

Figure 3.4.1 shows the relation between soil heat flux density at 0.01 m depth(G_2) and 0.03 m depth (G_1) and sensible heat flux density on the 3rd and 4th of August during the second observation period, which was characterized by the wet state of soil. The relation between soil heat flux of 0.01 m depth and sensible heat flux at the 0.45 m height from the ground surface can be given as;

$$H_e = 15.38 + 1.058\ G_2,\ r = 0.92 \tag{3.4.1}$$

Also the relation between soil heat flux density of 0.03 m depth and sensible heat flux density at the 0.45 m height from the ground surface can be expressed as;

$$H_e = 16.9 + 0.969\ G_1,\ r = 0.95 \tag{3.4.2}$$

The slope, interception and correlation coefficient are almost the same for equation (3.4.1) and (3.4.2). The daily maximum of soil heat flux was about 100 Wm^{-2} at two depths. These results indicate there is an appearance of thermally non-homogeneous soil layer i.e., quasi insulated layer between the soil surface and 0.03 m depth which is affected by the change of soil wetness.

Figure 3.4.2 shows the relationship between the soil heat flux and sensible heat flux during the second observation period on dry state of soil. The relation between the soil heat flux density of 0.01 m depth and that of 0.03 m depth and sensible heat flux density of 0.45 m height can be expressed respectively as;

$$H_e = 7.92 + 0.949\ G_2,\ r = 0.97 \tag{3.4.3}$$

$$H_e = 20.75 + 0.992\ G_1,\ r = 0.98 \tag{3.4.4}$$

Figure 3.4.2, equation (3.4.3) and (3.4.4), show that the slopes of relation curve are almost the same but the difference of interceptions is very large. Hence, line G_1 (soil heat flux of 0.03 m depth) looks

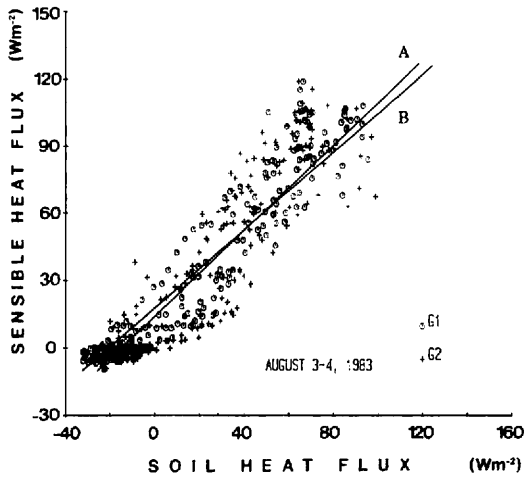

Figure 3.4.1. Relation between the sensible heat flux density at 0.45 m height from the ground surface and soil heat flux density. (Line A: G_2; 0.01 m depth, Line B: G_1; 0.03 m depth) on August 3−4, 1983.

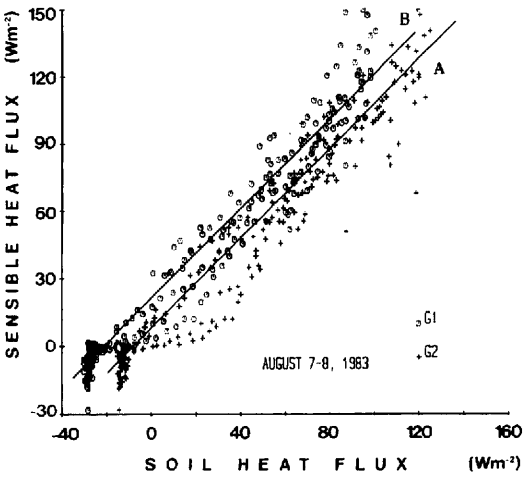

Figure 3.4.2 The same as the Figure 3.4.1, but for August 7−8,1983.

parallel to line G_2, shifted 20 Wm^{-2} towards the left.

Figure 3.4.3 shows the relation between soil heat flux density at 0.1 m depth and sensible heat flux density at 0.45 m height. Open circles represent the value observed under dry condition (i.e., for August 3 to 4) and cross symbols represent the value observed under wet condition (i.e., August 7 to 8). A hysteresis can be noticed in Figure 3.4.3. In another word, relation between G_{10} and H_e in the morning is different from that in the afternoon. This is due to the time lag of soil heat flux at 0.1 m depth. The soil heat flux in dry soil and in wet soil shows the same pattern. The range of time lag becomes smaller as the soil gets wetter. In spite of the difference in the maximum value of sensible heat for different

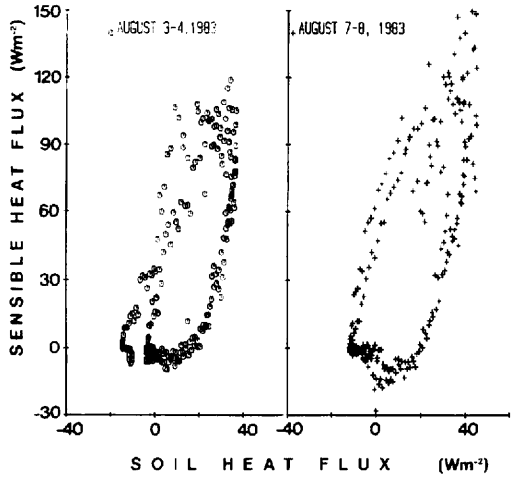

Figure 3.4.3. Relation between the sensible heat flux density and soil heat flux density at 0.1 m depth. (open circle; August 3-4, cross; August 7−8, 1983)

soil wetness, the maximum value of soil heat flux density is nearly the same.

3.5 Ratio R_n/I and soil moisture

It was examined how the wetness of soil affects the net radiation flux which is sometimes estimated from the solar radiative heat flux density. Figure 3.5.1 shows the relation between solar radiative heat flux density and net radiative heat flux density for the clear day of the first observation period. The correlation becomes higher when the data were classified based on the conditions of soil ($r=0.99$). The experimental formulae for each condition of soil moisture are as follows;

$$R_n = -1.4 + 0.61\ I,\ r = 0.99,\ 0.22 \leq \theta_w \leq 0.25 \tag{3.5.1}$$

$$R_n = -2.0 + 0.75\ I,\ r = 0.99,\ 0.30 \leq \theta_w \leq 0.44 \tag{3.5.2}$$

where θ_w is the volumetric soil water content of soil at the 0.02 m depth, and R_n, I are the net radiation and solar insolation, respectively.

The steeper slope for wet soil (0.75) as compared with that for dry soil (0.61) is due to the change of soil surface temperature and albedo in response to the wetness of soil moisture.

3.6 Drying process of soil moisture

Drying process of soil moisture from saturated equilibrium state is investigated in this subsection. In Figure 3.6.1, dotted lines, solied lines and closed circles indicate the time variations of the volumetric soil water contents at 0.01 m and 0.04 m depth and the difference between them, respectively. Soil moisture increases and/or decreases periodically within a day. The differences of soil moisture between two depths from 3 to 12 August are extremely large during the second observation period (Figure 3.6.2). The phase of volumetric soil water content variation is nearly consistent with that of soil temperature variation when the soil was wet on 3rd to 6th of August, 1983 in Figure 3.6.7. But the phase difference between the volumetric soil water content and the soil temperature variation increased as the

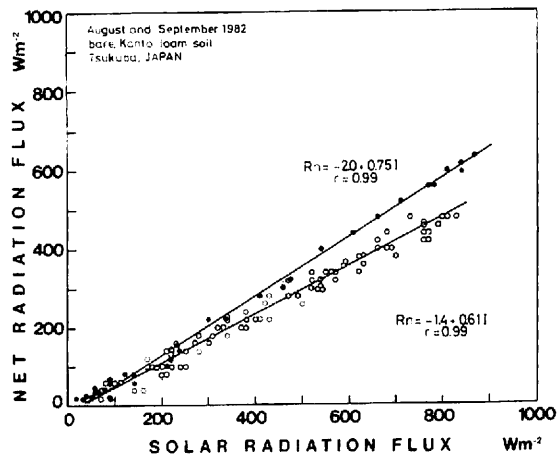

Figure 3.5.1. Relation between the net radiation flux and the solar radiation flux. Open and closed circles indicate the data obtained when the volumetric soil water content was in the range of 0.22−0.25 m^3m^{-3} and 0.30−0.44 m^3m^{-3} at 0.02 m depth, respectively.

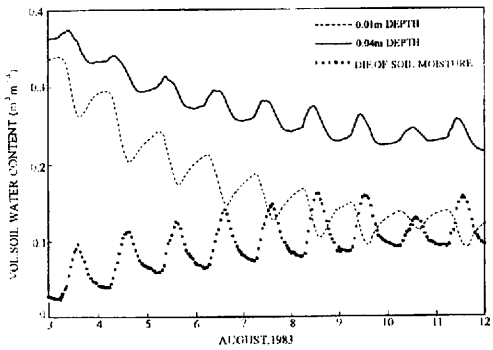

Figure 3.6.1 Daily variations of soil moisture and differences at two depths of 0.01 m and 0.04 m during August 3−12, 1983.

soil became dryer. Similarly, the phase difference is noticeable between soil moisture variations of 0.01 m and 0.04 m depth. The difference between volumetric soil water contents at 0.01 m and 0.04 m depth came up to maximum at around 15−16 hour which was the time when the soil moisture at 0.01 m became minimum. There is negative correlation between the difference and the volumetric soil water content at 0.01 m. On the other hand, it indicates a positive correlation between the difference of soil moisture and the volumetric soil water content at 0.04 m depth. Above results also represent the presence of the thermally insulated soil layer.

The volumetric soil water contents at depth of 0.01 m reveals the maximum value at 6−7 hour and the minimum value at 14−15 hour (Figure 3.6.3). On the other hand, the soil moisture at 0.04 m depth

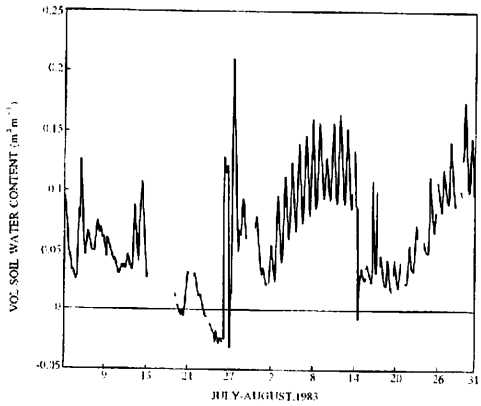

Figure 3.6.2 Daily variation of soil moisture differences between the depths of 0.01 m and 0.04 m during the second observation period.

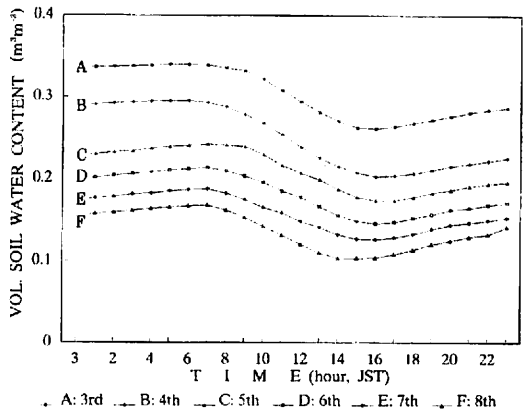

Figure 3.6.3 Diurnal variations of soil moisture at the depth of 0.01 m for 3 to 8 August, 1983.

reveals the maximum value at 10−12 hour and the minimum value at 19−20 hour (Figure 3.6.4). The soil moisture gradually decreases with time.

Figure 3.6.5 indicates the changing rate of soil moisture in an hour at 0.01 m depth. The positive and negative values of changing rate reveal the increment and decrement of soil moisture at that depth in an hour, respectively.

For 3 to 10 August, those figures reveal the pattern of gradual decrease of soil moisture during the daytime from the value of -0.014 $m^3m^{-3}h^{-1}$ to -0.01 $m^3m^{-3}h^{-1}$, and pattern of increase during nighttime from the value of 0.004 $m^3m^{-3}h^{-1}$ to 0.007 $m^3m^{-3}h^{-1}$. This means that there was deficiency of soil moisture at 0.01 m depth through the drying stage of soil moisture.

In Figure 3.6.6, the decreasing rates at 0.04 m depth during daytime varies from the value of -0.007 $m^3m^{-3}h^{-1}$ to -0.006 $m^3m^{-3}h^{-1}$ for 3 to 10, August, 1983. On the other hand, the rates of increment increased sharply during nighttime from 0.003 $m^3m^{-3}h^{-1}$ to 0.008 $m^3m^{-3}h^{-1}$. This means there was supply of soil moisture from the lower to the upper part of soil layer at 0.04 m depth.

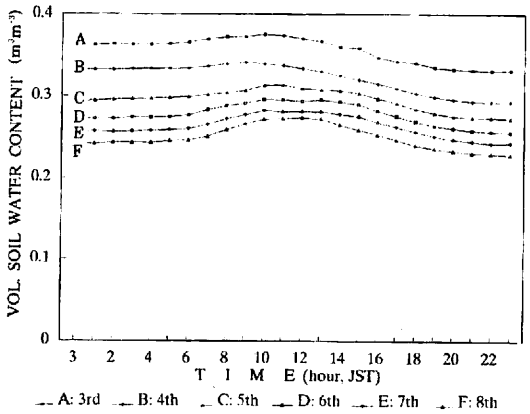

Figure 3.6.4 The same as the Figure 3.6.3 but for the depth of 0.04 m.

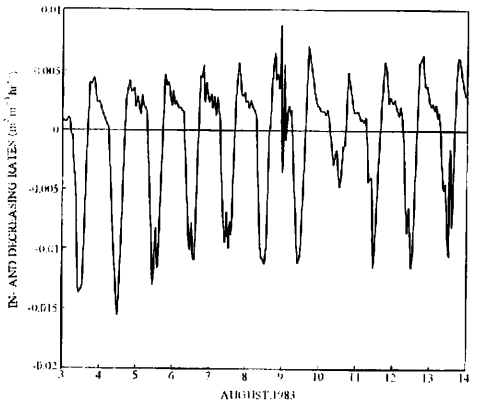

Figure 3.6.5 Daily variation of changing rates of the soil moisture at 0.01 m depth for 3 to 14, August, 1983.

The above findings and discussion can be summarized as follows.

(1) The volumetric soil water content at 0.01 m depth rapidly decreased as the soil temperature increased.

(2) Soil moisture at 0.04 m depth decreased slowly as the soil temperature increased.

(3) By the relationship (1) and (2), the difference between soil moisture at two depths became larger. We define this state as the forced evaporation stage.

(4) After sunset, the moisture flux from 0.04 m depth to 0.01 m depth exceeds the evaporation at surface. We also define this state as the soil moisture restore stage.

Figure 3.6.7 indicates the daily variations of soil temperature at each depth. Diurnal maximum soil temperatures at each depth decrease with increasing of soil moisture. In the Figure 3.6.7, diurnal maximum temperatures at 0.001m depth are larger than that of 0.05m or lower depth. From the above observation results, there is some what thermally different layer above and below of 0.02m depth. So we

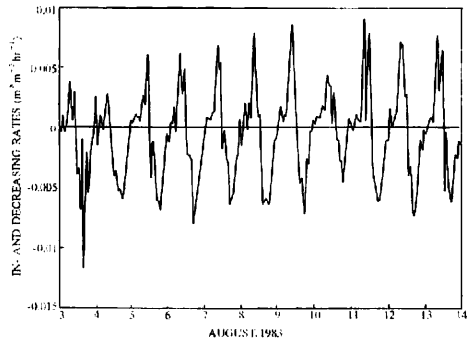

Figure 3.6.6 The same as the Figure 3.6.5 but for the depth of 0.04 m.

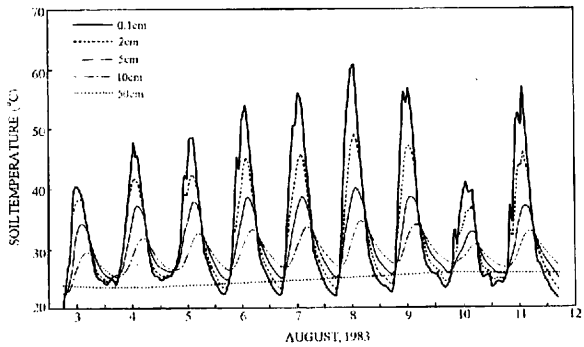

Figure 3.6.7 Daily variations of soil temperature at each depth at the second observation period.

call the soil surface layer to quasi insulated soil layer.

3.7 Energy balance components and soil moisture

To examine the effect of soil moisture on the energy balance and redistribution of solar energy on the bare soil surface, we suggest the use of the following parameters.

The equation (1.1.1) can be rewritten as follows;

$$L_n / Sn = 1 - R_n / S_n$$
$$= 1 - (H + lE + G) / S_n \quad (3.7.1)$$
$$S_n = S_d - S_u \quad (3.7.2)$$
$$L_n = L_d - L_u \quad (3.7.3)$$

where S_n and L_n indicate the net short wave radiation and net long wave radiation, respectively. The

net short wave radiation and net long wave radiation are precisely denoted by Kotoda (1986).

$$H_1 = L_n / S_n \tag{3.7.4}$$

$$H_2 = (H + lE + G) / S_n \tag{3.7.5}$$

$$H_1 + H_2 = 1 \tag{3.7.6}$$

$$H_r = H_1 / H_2,\ 0 \leq H_r \leq 1 \tag{3.7.7}$$

where H_1 is the ratio of long wave radiation to the net short wave radiation. H_2 is the ratio of summation of sensible heat energy, latent heat energy and soil heat energy to the net short wave radiation. Parameter H_r represents the ratio of H_1 and H_2. We define H_1 and H_2 as the radiative heat flux term and thermoand aerodynamic heat flux term, respectively. Consequently, the parameter H_r indicates the proportion of radiative heat flux term to the thermo-and aero-dynamic heat flux term in the energy balance.

In Chapter 2, a decreasing tendency of net radiation during the drying stage of soil moisture was observed (Figure 2.6.1). It is generally said that increase of the soil surface albedo causes the decrease of the net radiation. However, the net radiation is also a function of the soil surface temperature, and of incoming radiation components, we have to discuss them as well.

Figure 3.7.1 illustrates the variations of ratio R_n/S_n and of volumetric soil water content from 3 to 10 August, 1983. In the wet state of soil moisture from 3 to 5 August, the ratio of R_n/S_n was around 0.9 to 0.99. The ratio decreased down to 0.7−0.8 during 5 to 10 August when the soil moisture was below the value of 0.2 m^3m^{-3}. Thus, the R_n/S_n ratio is very large when the value of soil moisture is greater than 0.2 m^3m^{-3} at depth of 0.01 m. While the ratio gets smaller with decrease of soil moisture.

The ratio of H/S_n varied with soil moisture from 0.1 to 0.2 in the same duration. It shows the small increment of value of H/S_n with decreasing of soil moisture. This indicates that the absolute value of sensible heat energy is not large. However, the role of soil moisture on the sensible heat energy is large (Figure 3.7.2).

The ratio G_0/S_n shows a similar variation to the ratio of H/S_n. Figure 3.7.3 indicates the daily variation of the value of G_0/S_n during 3 to 10 August, 1983. The value of ratio varies from 0.1 to 0.22 with

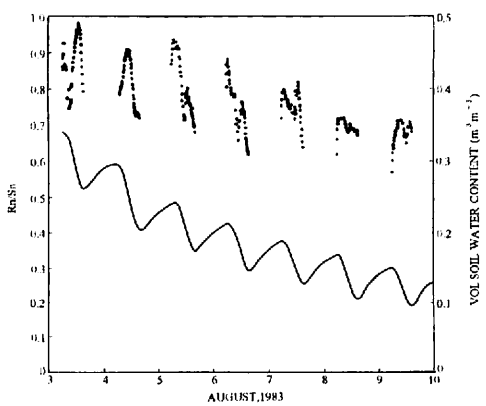

Figure 3.7.1 Daily variation of the ratio Rn/Sn and soil moisture from 3 to 10 August, 1983. Line and closed rectangle indicate the soil moisture and ratio R_n/S_n, respectively.

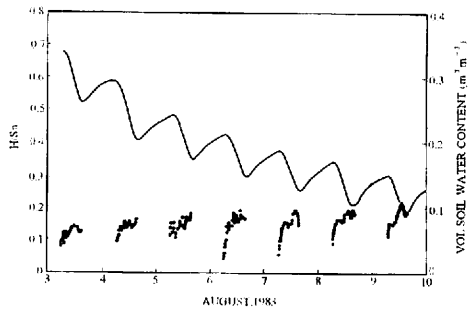

Figure 3.7.2 Daily variation of the ratio H/S_n and soil moisture from 3 to 10 August, 1983. Line and closed rectangle indicate the soil moisture and ratio H/S_n, respectively.

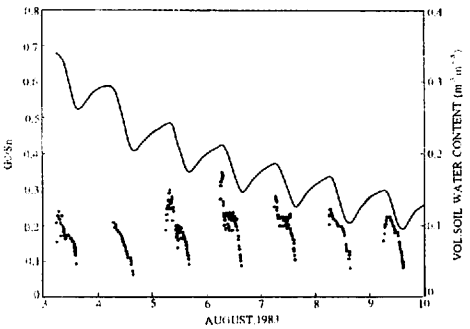

Figure 3.7.3 Daily variation of the ratio of G_0/S_n and soil moisture from 3 to 10 August, 1983. Line and closed rectangle indicate the soil moisture and ratio G_0/S_n, respectively.

decrease of the soil moisture. It can be said that the soil temperature gradient and soil thermal conductivity are compensated to each other.

Figure 3.7.4 illustrates the variations of the ratio lE/S_n and of soil moisture. The ratio lE/S_n varies with soil moisture from 0.6 at wet condition to 0.3 at dry state of soil moisture. This portion of latent heat flux on the energy balance is larger than other components.

The ratio L_n/S_n gradually increased from 0.1 to 0.35 with decrease of soil moisture. It reveals both increase of soil surface temperature and albedo with decrease of soil moisture (Figure 3.7.5).

The Bowen ratio (ß) which is widely used to estimate the evaporation is defined by

$$ß = H/lE \tag{3.7.8}$$

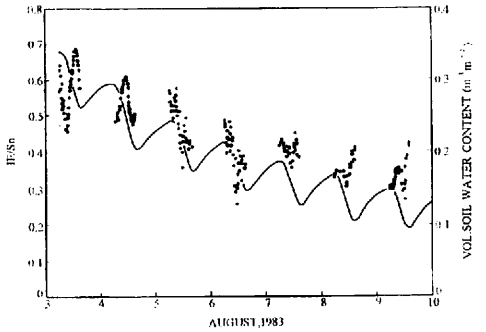

Figure 3.7.4 Daily variation of the ratio of lE/S_n and soil moisture from 3 to 10 August, 1983. Linc and closed rectangle indicate the soil moisture and ratio lE/S_n, respectively.

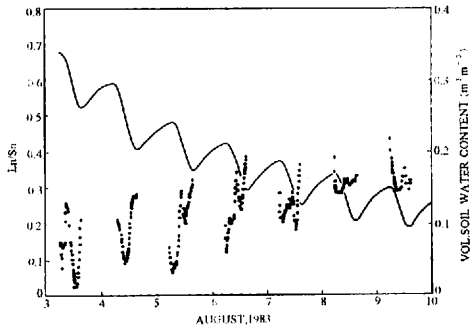

Figure 3.7.5 Daily variation of the ratio of L_n/S_n and soil moisture from 3 to 10 August, 1983. Line and closed rectangle indicate the soil moisture and ratio L_n/S_n, respectively.

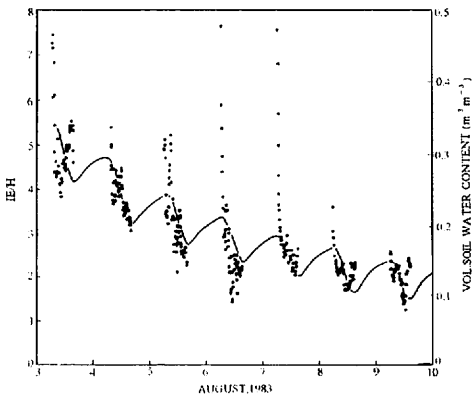

Figure 3.7.6 Daily variation of the ratio of lE/H and soil moisture from 3 to 10 August, 1983. Line and closed rectangle indicate the soil moisture and ratio lE/H, respectively.

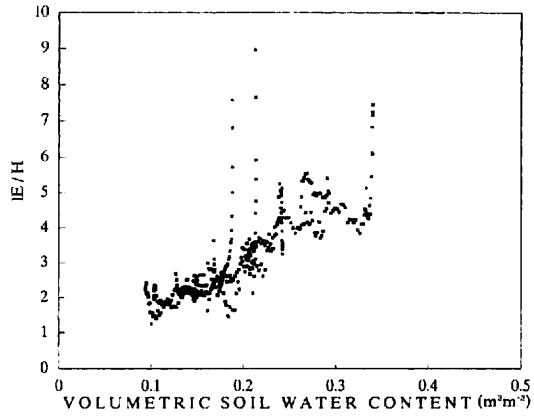

Figure 3.7.7 The ratio of lE/H versus soil moisture

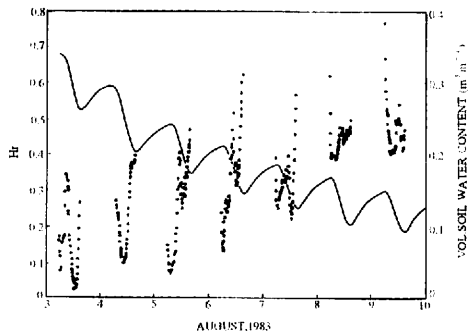

Figure 3.7.8 Daily variation of the parameter H_r and soil moisture from 3 to 10 August, 1983. Line and closed rectangle indicate the soil moisture and ratio lE/H, respectively.

To allow an easy comparison with the soil moisture variation, we use the inverse of Bowen ratio in this study. Figure 3.7.6 illustrates the variation of the inverse of Bowen ratio lE/H and soil moisture. It reveals a good correlation between the 1/ß and soil moisture. The values of 1/ß vary from 5 to 2 with drying of soil moisture.

Figure 3.7.7 represents the relationship between the inverse of Bowen ratio and volumetric soil water content during the second observation period. It reveals a good positive correlation between them.

Figure 3.7.8 indicate the variation of the parameter H_r and soil moisture on 3 to 10 August, 1983. The values increased from 0.1 to 0.5 with the decrease of soil moisture. This means that the net solar energy mainly transformed into sensible heat flux, latent heat flux and soil heat flux at wet state of soil moisture. On the other hand, the net solar energy onto the soil surface S_n is mainly changed into the

radiative heat flux term, i.e., upward long wave radiation at dry state of soil on 8 to 9 August. The value of H_r increases with decrease of soil moisture.

The relationship between the parameter H_r and volumetric soil water content are presented in Figure 3.7.9. It reveals the negative correlation.

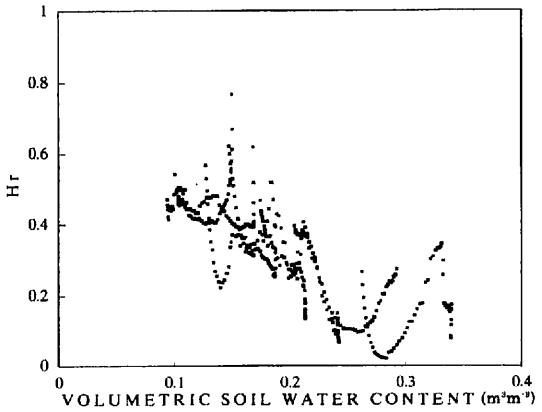

Figure 3.7.9 The parameter H_r versus soil moisture

CHAPTER 4

NUMERICAL EXPERIMENTS ON THE SOIL THERMAL CONDUCTIVITY OF KANTO LOAM

4.1 Finite difference equations

To investigate the effect of soil moisture which is related to the change of soil temperature, the differential equation for heat conduction was solved in the following. When it is assumed that there is no advection and conduction in the horizontal direction, the time change of the soil temperature can be expressed by

$$\partial T/\partial t = \partial (K_s \partial T/\partial z) /\partial z,\ K_s = K_{s(z)} = \lambda_{(z)}/C_{(z)} \tag{4.1.1}$$

where K_s is the soil thermal diffusivity, λ is the soil thermal conductivity, and $C_{(z)}$ is the heat capacity of soil. The general formula of the difference equation suggested by Richtmyer and Morton (1967) can be written as:

$$\frac{T_m^{n+1} - T_m^n}{\Delta t} = \frac{\theta\,[\delta (\sigma \delta T)]_m^{n+1} + (1-\theta)[\delta(\sigma\delta T)]_m^n}{(\Delta z)^2} \tag{4.1.2}$$

where $\sigma^{(n+1)} = \sigma^{(n)} = K_s$ and $\theta = 1/2$ were set, namely, Crank Niccolson Scheme was used. Then the equation becomes:

$$T_m^{n-1} - T_m^n = \frac{\Delta t}{2(\Delta z)^2} (\sigma_m + \tfrac{1}{2} T_{m-1}^{n+1} - \sigma_{m+\frac{1}{2}} T_m^{n+1} - \sigma_{m-\frac{1}{2}} T_m^{n+1}$$

$$+ \sigma_m \tfrac{1}{2} T_m^{n+1}{}_1 + \sigma_{m+\frac{1}{2}} T_{m+1}^n - \sigma_{m+\frac{1}{2}} T_{m-1}^n - \sigma_{m-\frac{1}{2}} T_m^n + \sigma_{m-\frac{1}{2}} T_{m-1}^n) \tag{4.1.3}$$

where n, m are numbers of time and depth direction in the grid numbers. Here the increasing amount of calculating depth is fixed as follows (Table 2).

Table 2 Depth and thickness of the soil layers used in the numerical experiments

LAYER NO	DEPTH (m)	THICKNESS (m)	LAYER NO	DEPTH (m)	THICKNESS (m)
1	0.0	0.012	11	0.216	0.038
2	0.012	0.013	12	0.254	0.043
3	0.025	0.015	13	0.298	0.048
4	0.041	0.017	14	0.346	0.054
5	0.058	0.019	15	0.401	0.061
6	0.077	0.021	16	0.462	0.068
7	0.099	0.024	17	0.53	0.077
8	0.123	0.027	18	0.608	0.086
9	0.151	0.03	19	0.694	0.097
10	0.181	0.034	20	0.791	0.108
			21	0.9	0.122

$$\log Z_i = 0.05i,\ i = 1, 2, 3, \ldots\ldots\ M$$
$$Z_i = 10.0^{0.05i} - 1$$
$$\Delta Z_i = Z_{i+1} - Z_i \tag{4.1.4}$$

Here we put the $\alpha_{(z)} = \sigma z * \Delta T/\Delta^2$, $\Delta T_m^n = T_{m+1}/2 - T_{m-1}/2$ into the equation (4.1.3). It can be arranged as:

$$-\alpha_{m+\frac{1}{2}} T_{m+1}^{n+1} + (2+\alpha_{m+\frac{1}{2}}+\alpha_{m-\frac{1}{2}}) T_m^{n+1} - \alpha_{m-\frac{1}{2}} T_{m-1}^{n+1} =$$
$$\alpha_{m-\frac{1}{2}} T_{m+1}^{n} + (2-\alpha_{m+\frac{1}{2}}+\alpha_{m-\frac{1}{2}}) T_m^{n} + \alpha_{m-\frac{1}{2}} T_{m-1}^{n} \tag{4.1.5}$$

When m which is from m = 1 to M is introduced into the equation (4.1.5), it will be:

for m = 1,
$$\{2 + (\alpha_{\frac{3}{2}} + \alpha_{\frac{1}{2}})\} T_1^{n+1} - \alpha_2 T_2^{n+1} = \alpha_{\frac{3}{2}} T_2^n + \{2 - (\alpha_{\frac{3}{2}} + \alpha_{\frac{1}{2}})\} T_1^n$$
m = 2,
$$-\alpha_{\frac{3}{2}} T_1^{n+1} + (2+\alpha_{\frac{5}{2}}+\alpha_{\frac{3}{2}}) T_2^{n+1} - \alpha_3 T_3^{n+1} = \alpha_{\frac{3}{2}} T_1^n + \{2 - (\alpha_{\frac{5}{2}}+\alpha_{\frac{3}{2}})\} T_2^n + \alpha_{\frac{5}{2}} T_3^n$$
m = 3,
$$-\alpha_{\frac{5}{2}} T_2^{n+1} + (2+\alpha_{\frac{7}{2}}+\alpha_{\frac{5}{2}}) T_3^{n+1} - \alpha_4 T_4^{n+1} = \alpha_{\frac{5}{2}} T_2^n + \{2 - (\alpha_{\frac{7}{2}} + \alpha_{\frac{5}{2}})\} T_3^n + \alpha_{\frac{7}{2}} T_4^n$$
m = 4,
$$-\alpha_{\frac{7}{2}} T_3^{n+} + (2+\alpha_{\frac{9}{2}}+\alpha_{\frac{7}{2}}) T_4^{n+1} - \alpha_5 T_5^{n-1} = \alpha_{\frac{7}{2}} T_3^n + \{2 - (\alpha_{\frac{9}{2}}+\alpha_{\frac{7}{2}})\} T_4^n + \alpha_{\frac{9}{2}} T_5^n$$
m = M − 1,
$$-\alpha_{M-\frac{3}{2}} T_{M-2}^{n+1} + (2+\alpha_{M-\frac{1}{2}} + \alpha_{M-\frac{3}{2}}) T_{M-1}^{n+1} = \alpha_{M-\frac{1}{2}} T_M^n + \{2 - (\alpha_{M-\frac{1}{2}} + \alpha_{M-\frac{3}{2}})\} T_{M-1}^n + \alpha_{M+\frac{3}{2}} T_{M-2}^n$$
m = M,
$$-\alpha_{M-\frac{1}{2}} T_{M-1}^{n+1} + (2+\alpha_{M+\frac{1}{2}}+\alpha_{M-\frac{1}{2}}) T_M^{n+1} = \{2 - (\alpha_{M+\frac{1}{2}}+\alpha_{M-\frac{1}{2}})\} T_M^n + \alpha_{M-\frac{1}{2}} T_{M-2}^n \tag{4.1.6}$$

When the above equation is converted to a tridiagonal matrix form, the equation will be:

$$\begin{bmatrix} 2+\alpha_{\frac{3}{2}}+\alpha_{\frac{1}{2}} & -\alpha_2 & & & & \\ -\alpha_{\frac{3}{2}} & 2+\alpha_{\frac{5}{2}}+\alpha_{\frac{3}{2}} & -\alpha_3 & & & \\ & -\alpha_{\frac{5}{2}} & 2+\alpha_{\frac{7}{2}}+\alpha_{\frac{5}{2}} & -\alpha_4 & & \\ & & -\alpha_{\frac{7}{2}} & 2+\alpha_{\frac{9}{2}}+\alpha_{\frac{7}{2}} & -\alpha 5 & \\ & & & \cdots\cdots & \cdots\cdots & \\ & & & -\alpha_{M-\frac{3}{2}} & 2+\alpha_{M-\frac{1}{2}}+\alpha_{M-\frac{3}{2}} & -\alpha_M \\ & & & & -\alpha_{M-\frac{1}{2}} & 2+\alpha_{M-\frac{1}{2}} \end{bmatrix} \begin{bmatrix} T_1^{n+1} \\ T_2^{n+1} \\ T_3^{n+1} \\ T_4^{n+1} \\ \cdots\cdots \\ T_{M-1}^{n+1} \\ T_M^{n+1} \end{bmatrix}$$
$$= \begin{bmatrix} \{2-(\alpha_{\frac{3}{2}}+\alpha_{\frac{1}{2}})\} T_1^n + \alpha_{\frac{3}{2}} T_2^n \\ \alpha_{\frac{3}{2}} T_1^n + \{2-(\alpha_{\frac{5}{2}}+\alpha_{\frac{3}{2}})\} T_2^n + \alpha_{\frac{5}{2}} T_3^n \\ \alpha_{\frac{5}{2}} T_2^n + \{2-(\alpha_{\frac{7}{2}}+\alpha_{\frac{5}{2}})\} T_3^n + \alpha_{\frac{7}{2}} T_4^n \\ \alpha_{\frac{7}{2}} T_3^n + \{2-\alpha_{\frac{9}{2}}+\alpha_{\frac{7}{2}}\} T_4^n + \alpha_{\frac{9}{2}} T_5^n \\ \cdots\cdots \\ \alpha_{M-\frac{1}{2}} T_M^n + \{2-(\alpha_{M-\frac{1}{2}}+\alpha_{M-\frac{3}{2}})\} T_{M-1}^n + \alpha_{M-\frac{3}{2}} T_{M-2}^n \\ \{2-(\alpha_{M-\frac{1}{2}})\} T_M^n + \alpha_{M-\frac{1}{2}} T_{M-1}^n \end{bmatrix} \tag{4.1.7}$$

where the equation (4.1.7) can be solved by Gauss-Seidel Elimination Method.

4.2 Initial and boundary conditions

Soil surface layer temperature observed at 0.001 m depth for every hour was used for the upper boundary condition. The boundary condition is specified in terms of the Fast Fourier Transform(FFT).

$$T_{(0,t)} = \frac{A_0}{2} + \sum_{n=1}^{L} [A_n cos\,(n\pi\frac{t}{L}) + B_n sin\,(n\pi\frac{t}{L})] \tag{4.2.1}$$

$$A_n = \frac{1}{L}\int_{-L}^{L} T_0(t) cos(n\pi\frac{t}{L})\,dt \tag{4.2.1a}$$

$$B_n = \frac{1}{L}\int_{-L}^{L} T_0(t) sin(n\pi\frac{t}{L})\,dt \tag{4.2.1b}$$

where L = 108. The result of FFT of the surface temperature during the whole calculation is shown in Figure 4.2.1. The lower boundary condition on the basis of the observed value is set as:

$$T_{(M,t)} = 25.0 \tag{4.2.2}$$

The initial condition is fixed as:

$$T_{(z(i),0)} = 20.7 + ((4.3/(z_{(M)} - z_{(i)}))*z(i), \tag{4.2.3}$$

$$i = 1,2,\ldots\ldots, M-1.$$

4.3 Estimation of soil thermal conductivity

The equation which reveals the relation between the volumetric soil water content and soil thermal conductivity was formulated as the following. The value was read on coordinates from Figure 4.3.1. Namely, the equation of soil thermal conductivity of loam (porosity, 0.41) suggested by Kimball et al. (1976) is expressed as follow:

$$\lambda_{ki(z,t)} = 4.038\ \theta_{w(z,t)} + 0.865 \tag{4.3.1}$$

And of peat soil(porosity, 0.8) suggested by Kersten (1949) can be expressed as:

$$\lambda_{ke(z,t)} = 0.509\ \theta_{w(z,t)} + 0.033 \tag{4.3.2}$$

where λ_{ki}, λ_{ke} mean the soil thermal conductivity for loam and peat, respectively, and θ_w the volumetric soil water content. The volumetric soil water content used here was estimated in Chapter 3.1 as Figure 3.1.1.

The changing pattern of the soil thermal conductivity as a function of time is shown in Figure 4.3.2 and Figure 4.3.3. Figure 4.3.2 shows the change of soil thermal conductivity of loam which is derived from the equation (4.3.1) near the soil surface. As in Figure 4.3.2, thermal conductivity decreases as the decrease of volumetric soil water content near the soil surface so that it shows about 0.5 − 1.5 $Wm^{-1}K^{-1}$. As the depth of soil becomes deeper, the decrease of the gradient becomes gentle so it shows 1.3 − 1.8 $Wm^{-1}K^{-1}$ at 0.1m depth.

Also Figure 4.3.3 is the result derived from the equation (4.3.2). Even the soil thermal conductivity

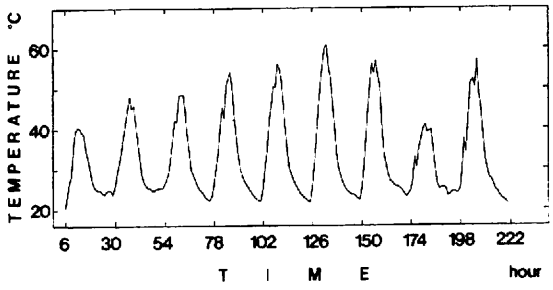

Figure 4.2.1 Variation of surface soil layer temperature interpolated by the Fast Fourier Transform.

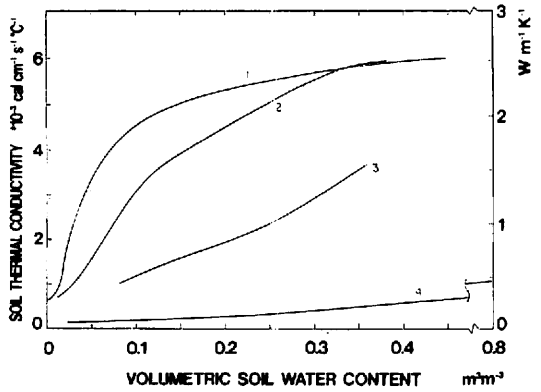

Figure 4.3.1. Thermal conductivity λ of four types of soils as functions of volumetric soil water content θ_w (referred from Brutsaert, 1981); Curve 1 represents laboratory results on a quartz sand (Porosity 0.43) obtained by De Vries (1963); Curve 2 represents laboratory data on a sand loam (porosity 0.38) of Moench and Evans (1970); Curve 3 is the median line through field data on a loam (mean porosity 0.41) from Kimball et al. (1976); Curve 4 represents laboratory data on a peat soil (porosity around 0.8) from Kersten (1949).

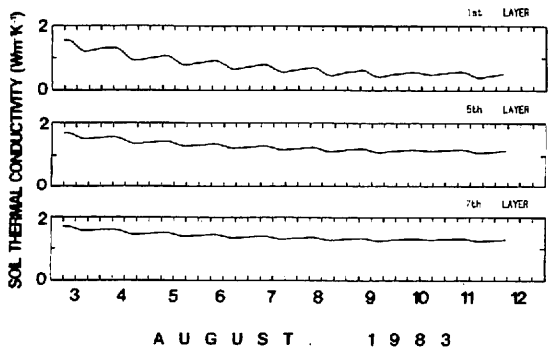

Figure 4.3.2 Estimated thermal conductivity λ_{ki} (porosity 0.41) at surface layer (1st layer), 0.058m depth (5th layer), 0.099 m depth (7th layer).

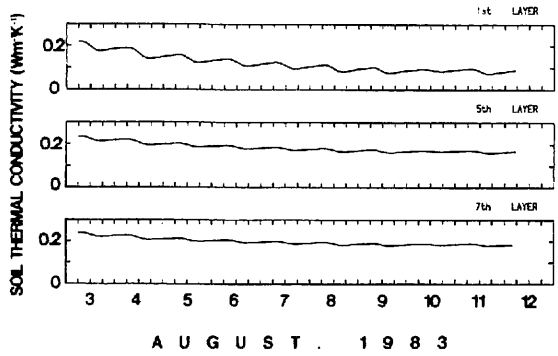

Figure 4.3.3 The same as the Figure 4.3.2 but for the λ_{ke} of peat soil (porosity 0.8).

decreases as the soil moisture decreases near the surface, the heat conductivity in loam which is about 0.1 – 0.22 $Wm^{-1}k^{-1}$ is five or six times larger than that in peat soil.

4.4 Estimation of soil thermal diffusivity

It has been studied about diffusivity of sensible heat flux density and latent heat flux density within the surface boundary layer in detail (Yaglom, 1977; O'Brien, 1970). On the other hand, soil thermal diffusion coefficient is approximately considered as constant on a function of depth and time since it is regarded that the soil moisture is constant and soil heat flux density is not so big as sensible heat flux density, latent heat flux density and radiation flux density in atmosphere. However, it has to be treated as a variable of depth and time when it changes as a function of time and space as in this paper. Therefore, soil thermal diffusion coefficient was obtained by the following calculation;

$$\begin{aligned} K_{s(z,t)} &= \lambda / C_s, \\ \lambda &= \lambda_{(\theta w,z,t)} \\ C_s &= C_{s(\theta w,z,t)} \end{aligned} \qquad (4.4.1)$$

where Cs is the volumetric soil thermal capacity. A knowledge of the volume fractions of mineral soil, θ_m, organic matter θ_c, volumetric soil water content θ_w, and fraction of air θ_a, allows the determination of the volumetric soil thermal capacity as follows (Brutsaert, 1981)

$$C_s = \rho_m\, \theta_m\, c_m + \rho_c\, \theta_c\, c_c + \rho_w\, \theta_w\, c_w + \rho_a\, \theta_a\, c_a \qquad (4.4.2)$$

where the c terms are the specific heats and the ρ terms the densities as indicated by the subscripts. De Vries (1963) suggests the volumetric soil thermal capacity in ($Wm^{-3}K^{-1}sec$) as follows

$$C_s = (1.94\ \theta_m + 2.50\ \theta_c + 4.19\ \theta_w) \times 10^6 \qquad (4.4.3)$$

The fraction of organic matter was 0.01, and the volumetric soil water content estimated from equation (3.1.5) was used. The fraction of soil mineral on the Kanto loam was reported as 0.3 by Shimada et al. (1992), and 0.2 by Tanaka (1980) and Hwang (1989). In this study, the volume fraction of solid soil

was adopted as 0.2.

Figure 4.4.1 shows the variation of soil thermal diffusion coefficient calculated by introducing the equation of Kimball et al. (1976) (λ_{ki} will stand for this equation afterwards). In Figure 4.4.2, Kersten(1949) equation (λ_{ke} will stand for this equation afterwards) was introduced into the Equation 4.4.1. The soil thermal diffusion coefficient near the surface has approximately the range of $7.5*10^{-7} - 9*10^{-7}$ m^2sec^{-1} and it is decreasing as time passes with diurnal change. It even decreases at 0.06m depth and maintains almost constant value of $9*10^{-7}$ m^2sec^{-1} at 0.1m depth. It is fixed to the extent of $1.3*10^{-7}$ m^2sec^{-1} near the surface through the whole calculation period and is somewhat decreasing as time passes in Figure 4.4.2.

Figure 4.4.3 and Figure 4.4.4 illustrate the soil thermal diffusion coefficients at 6 hour and 14 hour which are the daily minimum and maximum soil temperature respectively as a function of depth. Diffusion coefficients were obtained by Figure 4.4.3 and Figure 4.4.4. It is decreasing near the surface as soil moisture decreases in Figure 4.4.3, and also it shows the decreasing pattern as in Figure 4.4.4.

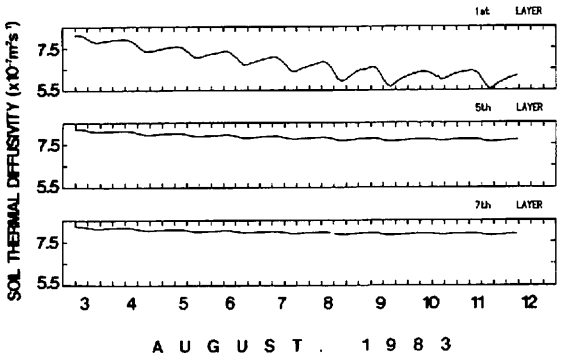

Figure 4.4.1 Estimated soil thermal diffusivity K_s of loam (porosity 0.41). Each depth are the same as the Figure 4.3.3.

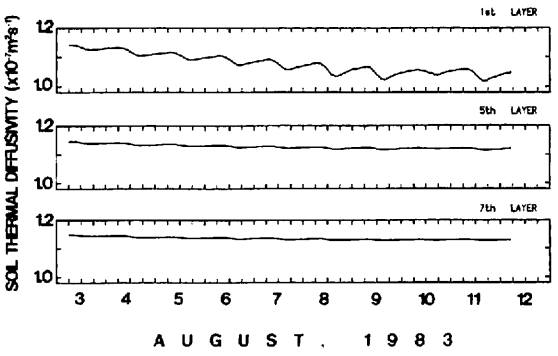

Figure 4.4.2 The same as the Figure 4.4.1, but for peat soil (porosity 0.8).

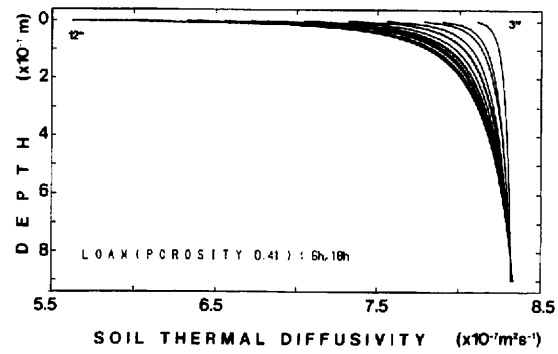

Figure 4.4.3 Profiles of estimated soil thermal diffusivity of loam (porosity 0.41) on 6 hour and, 18 hour 3−12 August 1983.

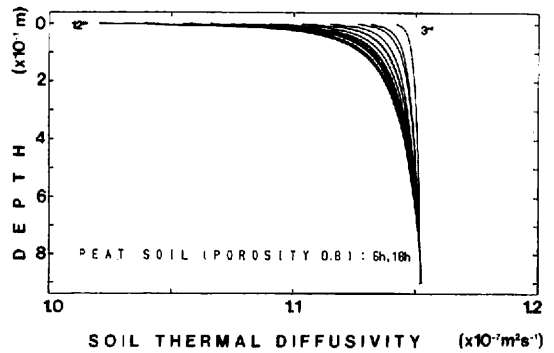

Figure 4.4.4 The same as the Figure 4.4.3, but for the peat soil (porosity 0.8).

4.5 Comparison between the calculated and observed soil temperature

To investigate the effect of soil moisture which has influenced on the soil temperature which varies in time and depth, numerical experiments on the soil temperature were carried out with the interval of 600 second from 6 hour of August 3rd (starting time; 6 hour) to 6 hour of August 12th (ending time; 222 hour) by using the difference equation. Daily variation of the calculated soil temperature is illustrated from 6 hour of August 8th to 6 hour of August 9th in Figure 4.5.1 and in Figure 4.5.2. Figure 4.5.1 and 4.5.2 are the result of using λ_{Ki} and λ_{Ke}, respectively. When the soil surface temperature changes from about 21℃ to 62℃, the soil temperature of a function of time varies with depth from the surface to 0.5 m depth. But there is no variation underneath the depth, which is accord to the real observation value in Figure 4.5.3. In spite of the same surface temperature, there is no soil temperature variation using the soil conductivity λ_{Ke} from 0.2 m depth and temperature profile is a lot different from the observed value. Figure 4.5.4 illustrates the time change of the calculated soil temperature at 0.058 m depth through whole calculation period. To compare with this, the observed value at 0.05 m depth is illustrated at the same time in curve 1. Curve 2 and 3 in the Figure 4.5.4 are the time change of the calculated value of the soil temperature that is referred the heat conductivity λ_{Ki} and λ_{Ke}, respectively. Figure

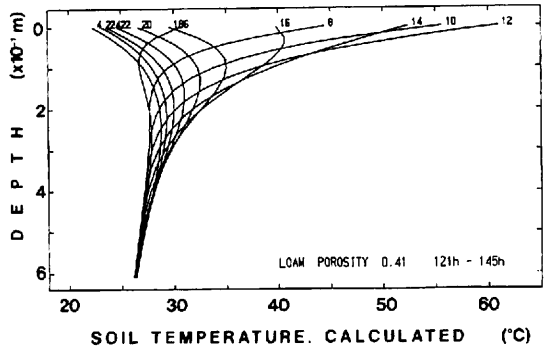

Figure 4.5.1 Calculated Tautochrones of loam on 8 August 1983

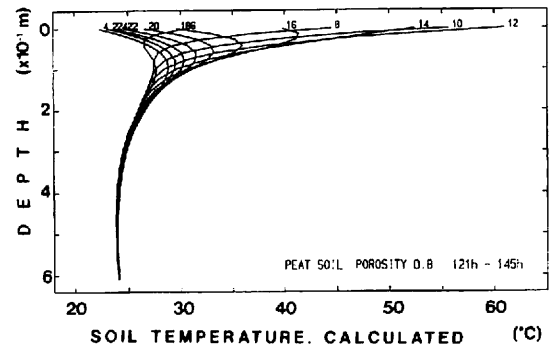

Figure 4.5.2 Calculated Tautochrones of peat soil on 8 August 1983.

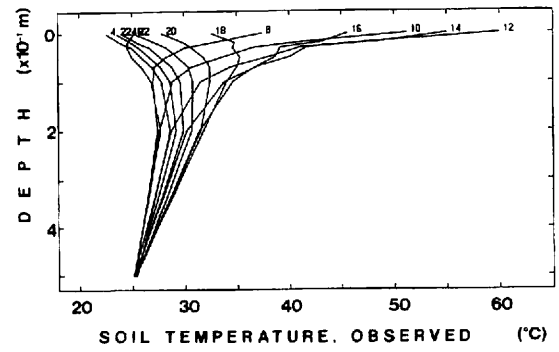

Figure 4.5.3 Observed Tautochrones of Kanto loam (porosity 0.8) on 8 August 1983.

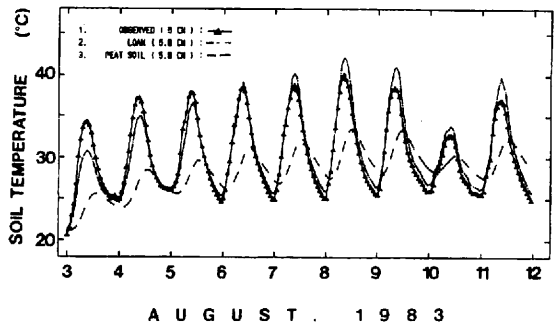

Figure 4.5.4 Variations of soil temperature observed at 0.05 m depth and calculated at 0.058 m depth through 3−12 August 1983.

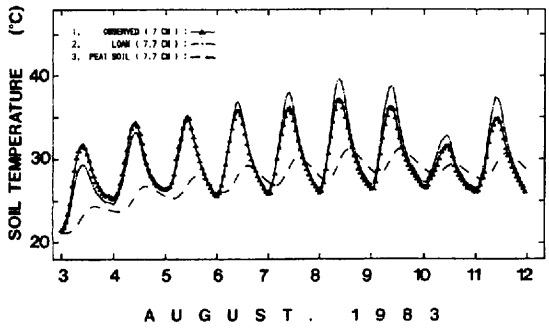

Figure 4.5.5 Variations of soil temperature observed at 0.07 m depth and calculated at 0.077 m depth through 3−12 August 1983.

4.5.5 also shows the time variation of observed and calculated soil temperature. The line 1 illustrates the observed soil temperature at the depth of 0.07 m, and line 2 and 3 show the calculated soil temperature at the 0.077 m of calculating depth using the soil thermal conductivity λ_{Ki} and λ_{Ke} which referred from the Figure 4.3.1, respectively.

As shown in the Figure 4.5.4 and Figure 4.5.5, the calculated soil temperature using the λ_{Ki} is closer to the observed value than that of using the λ_{Ke}. The calculated temperature of curve 2 and the observed one well coincide with each other when the daily minimum soil temperature appears. In the case of daytime, the tendency of variation and relative value of soil temperature show good coincidence with observed value. By the way, the calculated value of soil temperature is under estimated at the beginning of the calculation, namely, the wet state of soil. On the other hand, it is over estimated at the dry state of soil. The difference between the calculated and observed value may be come about by the soil thermal conductivity and diffusivity which are estimated from soil moisture profile. It means that the estimation of soil moisture profile by using the logarithmic distribution is not complete yet.

4.6. Discussion on the results of the numerical experiments

For the estimation of soil temperature variation by the use of numerical simulation, the soil thermal conductivity and diffusivity in the equation 4.4.1 must be taken as a variable of depth and time. But

many of researches studied about the soil temperature dealt the soil thermal conductivity and diffusivity as a constant.

In this study, the soil thermal conductivity and diffusivity are taken into numerical experiment as a function of soil moisture which varied with depth and time, and which are interpolated by use of Fast Fourier Transform. Especially, the soil moisture are assumed to be a logarithmic distribution with depth, namely, the soil moisture is logarithmically decreased with depth in the soil.

This conception means that the uppermost part of soil layer has a little soil moisture and has a characteristic of quasi insulated layer which shows low thermal conductivity.

The followings have been perceived by the result of the numerical experiments on soil temperature:

1) It is considerably valid for the numerical experiments on soil temperature that the distribution of soil moisture is assumed to be a logarithmic profile by the comparison with the observed data.
2) The heat conductivity of Kanto loam is comparable to the value of loam with 0.41 porosity rather than to the value of peat soil with 0.8 porosity. Hence, the heat conductivity of the studied area is close to $\lambda_{(z,t)} = 4.0380\ \theta_{w(z,t)} + 0.865\ \mathrm{Wm^{-1}K^{-1}}$.
3) Soil thermal diffusivity of study area of Kanto loam are the range of $7.5\times10^{-7} - 9\times10^{-7}\ \mathrm{m^2sec^{-1}}$.

CHAPTER 5

CONCLUSIONS

The effect of soil moisture on the energy balance at the surface of a bare soil and on soil temperature was investigated by means of field observations and numerical experiments. The principal findings on the mechanisms through which the soil temperature and energy balance are influenced by the daily soil moisture variation are as follows.

Consider a state of a bare soil surface initially saturated by precipitation. As the precipitation ceases, the soil moisture in the upper most part of the soil layer will be evaporated by the radiative heat energy, which is thus mainly transformed into latent heat flux. As time proceeds, the evaporating moisture will play a major role in determination the surface temperature. We may classify the controlling mechanisms into two parts, namely, those acting during daytime and those acting during nighttime.

First of all, the mechanisms controlling daytime energy balance may be described as follows;

(A) The soil moisture in the uppermost part of soil layer can be expected to be vigorously evaporated by the radiative heating energy (mainly solar insolation energy).

(B) In response to the drying of the soil layer by the process described in (A), an increase in the albedo of the soil, a decrease of the soil thermal conductivity and a decrease of the soil heat capacity take place.

(C) The quasi insulated soil layer becomes evident in the uppermost part of the soil with a depth of about 0.01 m by the effect of the decreasing the soil thermal conductivity.

(D) A geo-thermocline, which is situated under the quasi insulated soil layer, becomes established at a depth of about $0.01-0.02$ m.

This process results in a steeper gradient of surface soil temperature just below this layer. As a result, the heat flux into the soil increases. It also results in an increase of the ratio of G/R_n (soil heat flux / net radiation). Similarly, the steeper air temperature gradient near the soil surface contributes to the formation of unstable stratification of lower atmospheric layer.

In the second place, the night time mechanisms can be described as follows;

(E) The evaporating process of soil moisture is weakened at nighttime. Within one to two hours after sunset, the quasi insulated layer disappears by the supply of moisture from the lower layers.

(F) As time goes on, the daytime soil moisture loss of the uppermost part is eventually at least partially compensated by the supply of moisture from the lower soil layers.

(G) As a result of (F), an increase in the heat capacity and in the thermal conductivity of the soil can be expected, and the soil heat diffusion coefficient increases.

(H) As a result of (G), the quasi insulated soil layer disappears.

(I) As a result of (H), it can be expected that the outgoing heat flux from soil layer increases and the downward sensible heat flux decreases. Consequently, the rate of G_1/R_n (soil heat flux / net radiation) is bound to increase.

From the above results and discussion, the following can be concluded:

1). There is a low heat conducting layer near the soil surface under dry conditions in the study area of Kanto loam. This layer can be defined as a quasi insulated soil layer which can be assumed to develop from the soil surface down to lower depth of about 0.01 m; this depth tend to increase with the drying of the soil. The quasi insulated soil layer reveals the following characteristics.

(1) The volumetric soil water content in the layer can be as low as 0.1 to 0.2 m^3m^{-3}.

(2) It reveals high rates of change of soil temperature, and these rates may vary from 5℃ h^{-1} to 10℃ h^{-1}.

(3) The soil temperature gradient in the quasi insulated soil layer is very steep with typical value of $5x10^2$℃ m^{-1}–$7x10^2$℃ m^{-1}.

2). When the soil surface in a moist state, the incident solar energy onto the bare surface is mainly redistributed into the thermo-and aerodynamic heat flux terms, namely, sensible heat flux, latent heat flux, and soil heat flux. On the other hand, it is mainly transformed into a long-wave radiative heat flux when the soil is dry.

When the volumetric soil water content at 0.01 m varies from 0.35 m^3m^{-3} to 0.1 m^3m^{-3}, namely, from a wet to a dry state, each component of the energy balance typically varies as follows.

(1) The ratio of net radiation and net short wave radiation R_n/S_n decreases from 0.9 to 0.7.

(2) The ratio of sensible heat flux and net short wave radiation H/S_n, and the ratio of soil heat flux at soil surface and net short wave radiation G_0/S_n increases from 0.1 to o.2.

(3) The ratio of latent heat flux and net short wave radiation lE/S_n decreases from 0.6 to 0.3.

(4) The ratio of net long wave radiation and net short wave radiation L_n/S_n increases from 0.1 to 0.3.

(5) The ratio of latent heat flux and sensible heat flux lE/H, which is the inverse of the Bowen ratio, decreases from 5 to 2.

(6) The parameter H_r which is the ratio of radiative heat flux term to the thermo- and aerodynamic heat flux term increases from 0.1 to 0.5.

3). In the numerical experiments on the soil temperature variation, the soil thermal conductivity and diffusivity must be dealt with as functions of soil moisture which vary with depth and time. The profile of soil moisture can be assumed to increase logarithmically with depth from the soil surface. The model's output of soil temperature reveals good agreement with the observational results. This confirms the presence of quasi insulated soil layer in the upper most part of the soil.

REFERENCES

Ågstrom, A. (1925): The albedo of various surfaces of ground. Geografiska Annaler, 7, 323−342.

Begg, J. E., J. F. Bierhuizen, E. R. Lemon, D. K. Misra, R. O. Slatyer, and W. R. Stern (1964): Diurnal energy and water exchanges in Bulrush millet in an area of high solar radiation, Agr. Meteor., 1, 294-312.

Bristow, K. L. (1987): On solving the surface energy balance equation for surface temperature, Agri. and Forest Meteo., 39, 49−54.

Brunt, D. (1932): Notes on radiation in the atmospere, Quart. J. Roy. Meteor. Soc., 58, 389−420.

Brutsaert, W. (1981): Vertical flux of moisture and heat at a bare soil surface, 115−168, in Eagleson, P. S. (ed), "Land surface processes in atmospheric general circulation models". Cambridge University Press, London, 560p.

Camillo P. J., R. J. Gurney and T. J. Schmugge (1983): A soil and atmospheric boundary layer model for evapotranspiration and soil moisture studies, Water Resources Research, 19, 371−380.

Choudhury, B. J. and J. L. Monteith (1988): A four-layer model for the heat budget of homogeneous land surfaces, Quart. J. Roy. Meteor. Soc., 114, 373 398.

Davies, J. A. and P. H. Buttimor (1969): Reflection coefficients, heating coefficients and net radiation at Simcoe, Southern Ontario, Agr. Meteor., 6, 373−386.

Deardorff, J., W. (1978): Efficient prediction of ground surface temperature and moisture, with inclusion of a layer of vegetation, Jour. of Geophysical Research, 83, 1889−1903.

De Vries, D. A. (1963): Thermal properties of soil, 210-235, Ch. 7 in Van Wijk, W. R. (Ed.), "Physics of plant environment", North-Holland Pub. Co., Amsterdam, 382pp.

Durand, P., Frangi, J. P. and Druilhet, A. (1988): Energy budget for the Sahel surface layer during the ECLATS experiment. Boundary-layer Meteorology, 42, 27−42.

Graser, E. A. and C. H. M. Van Bavel (1982): The effect of soil moisture upon soil albedo. Agr. Meteor. 27, 17−26.

Hayashi Y., S. J. Hwang (1981): Characteristics of wind speed and friction velocity observed by the cup-anemometer and sonic anemometer thermometer. Bulletin of the Environmental Research Center, Uni. Tsukuba, 5, 1−10.

Hwang, S. J. (1989): A study on the numerical experiment of the soil temperature, Jour. Science, Pusan Univ., 48, 139−159.

Idso, S. B. and K. R. Cooly (1971): The vertical location of net radiometers, I. The effects of the underlying air layer, Jour. Meteor. Soc. of Japan, 49, 343−349.

Idso, S. B., R. D. Jackson, R. J. Resinato, B. A. Kimball and F. S. Nakayama (1975): The dependence of bare soil albedo on soil water content, Jour. Appl. Meteor., 14, 109−113.

Kayane I. (1980): Hydrology, Taimeido, Tokyo, 272p. (Japanese)

Kersten, M. S. (1949): Thermal properties of soils, Bull. Univ. Minnesota Inst. of Techn. Engin. Exper. Stst., 28, 227p.

Kimball, B. A., R. D. Jackson, R. J. Reginato, F. S. Nakayama and S. B. Idso (1976): Comparison of field-measured and calculated soil heat fluxes. Soil Sci. Soc. Amer. Jour., 40, 18−25.

Kondo, J. and N. Saigusa (1992): A model and experimental study of evaporation from bare-soil surfaces. Jour. of Appl. Meteor. 31, 104 -112.

Kotoda, K. (1986): Estimation of river basin evapotranspiration, Environ. Res. Cent. Papers, 8, 66pp.

Kuo, H. L. (1968): The thermal interaction between the atmosphere and the earth and propagation of diurnal temperature waves, Jour. Atmos. Sci., 25, 682−706.

Mahrer, Y. and M. Segal (1985): Model evaluations of the impact of perturbed weather conditions on soil-related characteristics, Soil Science, 140, 368−375.

Moench, A. F. and D. D. Evans (1970): Thermal conductivity and diffusivity of soil using a cylinderical heat source, Soil Sci. Soc. Amer. Proc., 34, 377−381.

O'Brien, J. (1970): On the vertical structure of the eddy exchange coefficient in the planetary boundary layer, Jour. Atmos. Sci., 27, 1213−1215.

Philip, J. R. (1957): Evaporation, and moisture and heat field in the soil. Jour. Meteor., 14, 354−366.

Rakovec J. and A. Hocevar (1988): Simulation of soil−and airmicroclimate modifications using soil heating with warm water, Agri. and Forest Meteo., 42, 41−52.

Richtmyer, R. O. and K. W. Morton (1967): Difference methods for initial value problems, Inter-science Publishers, New York, 405p.

Rosenberg, N. J. (1966): Microclimate, air mixing and physiological regulation of transpiration as influenced by wind shelter in an irrigated bean field, Agr. Meteor., 3, 197−224.

Sasamori T. (1970): A numerical study of atmospheric and boundary layers, Jour. Atmos. Sci., 27, 1122 -1137.

Schieldge J. P., A. B. Kahle and R. E. Alley (1982): A numerical simulation of soil temperature and moisture variations for a bare field, Soil Science, 133, 197−207.

Schmugge, T. T., T. J. Jackson, H. L. McKim (1980): Survey of methods for soil moisture determination, Water Resources Research, 16, 961−979.

Shimada, J., R. Kawamura, M. Taniguchi, and M. Tsujimura (1992): Continuous soil moisture content measurement at the experimental field of ERC by using the heat-probe type soil moisture sensor. Bulletin of the Environmental Research Center, Uni. Tsukuba, 16, 45−53.

Stanhill, G., G. J. Hofstede, and J. D. Kalma (1966): Radiation balance of natural and agricultural vegetation, Quart J. Roy. Meteor. Soc., 92, 128−140.

Tanaka T. (1980): Soil water characteristics and specific yield of Kanto loam and Imaichi district, Tochigi prefecture, Geogr. Rev. of Japan, 53, 646−665.

van Bavel, C. H. M. and L. J. Fritschen (1965): Energy balances of bare surfaces in an arid climate, UNESCO, Methodology of plant Eco-physiology, Proc. of the Montpellier Symp., 99 - 107.

Yaglom, (1977): Comments on wind and temperature flux profile relationship, Boundary Layer Meteor., 11, 89−102.

Environmental Research Center Papers

No.1 (1982) Kenji KAI: Statistical characteristics of turbulence and the budget of turbulent energy in the surface boundary layer. 54p.

No.2 (1983) Hiroshi IKEDA: Experiments on bedload transport, bed forms, and sedimentary structures using fine gravel in the 4-meter-wide flume. 78p.

No.3 (1983) Yousay HAYASHI: Aerodynamical properties of an air layer affected by vegetation. 54p.

No.4 (1984) Shinji NAKAGAWA: Study on evapotranspiration from pasture. 87p.

No.5 (1984) Fujiko ISEYA: An experimental study of dune development and its effect on sediment suspension. 56p.

No.6 (1985) Akihiko KONDOH: Study on the groundwater flow system by environmental tritium in Ichihara region, Chiba Prefecture. 59p.

No.7 (1985) Chong Bum LEE: Modeling and climatological aspects of convective boundary layer. 63p.

No.8 (1986) Kazuo KOTODA: Estimation of river basin evapotranspiration. 66p.

No.9 (1986) Abdul Khabir ALIM: Experimental studies on transient behavior of capillary zone. 76p.

No.10 (1987) Michiaki SUGITA: Evaporation from a pine forest. 61p.

No.11 (1987) Hye-Sock PARK: Variations in the urban heat island intensity affected by geographical environments. 79p.

No.12 (1988) Hiroshi IKEDA and Fujiko ISEYA: Experimental study of heterogeneous sediment transport. 50p.

No.13 (1990) Hitoshi TORITANI: A local climatological study on the mechanics of nocturnal cooling in plains and basins. 62p.

No.14 (1990) Ryuichi KAWAMURA: Large-scale air-sea interactions in the tropical western Pacific on interannual and intraseasonal time scales. 64p.

No.15 (1992) Yoshinori KODAMA: Effect of abrasion on downstream gravel-size reduction in the Watarase River, Japan: Field work and laboratory experiment. 88p.

No.16 (1993) Isamu KAYANE, Hironobu OGASAWARA and Makoto YOSHIDA: Four-dimensional response of the aquifer and aquitard system in Tokyo to groundwater withdrawal and regulation. 53p.

No.17 (1995) Soo-Jin HWANG: The effect of soil moisture on the energy balance at the bare soil surface. 51p.

発行　　平成7年12月27日

編集・発行者　筑波大学水理実験センター

〒305 つくば市天王台1－1－1

TEL 0298(53)2532 FAX (53)2530

印刷　ニッセイエブロ株式会社

東京都港区西新橋2－5－10